

## Selection of slip systems in confined single crystal gradient plasticity: coupled effects of slip system orientations, latent hardening, and grain boundaries

J. L. DEQUIEDT

*CEA, DAM, DIF, 91297 Arpajon, France, e-mail: jean-lin.dequiedt@cea.fr*

IN CRYSTAL PLASTICITY UNDER PRESCRIBED DEFORMATION, the incremental material response is potentially non-unique owing to slip system redundancy for most of the crystalline structures. Following Petryk, energy minimizing considerations give the way to select one of these solutions and the set of active systems, which depend on their more or less favorable orientation and their mutual interactions (latent hardening). This variational approach is extended here to confined plasticity in a finite volume, simulating a single crystal embedded in an aggregate. A slip gradient enhanced framework and related micro-hard boundary conditions are considered, using two defect energies introduced by Gurtin and coworkers: the first one takes the slip system polar dislocation densities as internal state variables and the second one is a quadratic potential of the dislocation density tensor. In both cases, micro-hard conditions amount to null flow for the two former quantities. For the classical one dimensional case of a strip in simple shear, the two models yield substantially different solutions, the second one coupling the gradients on the different systems. These results emphasize the necessity for a physically motivated modeling of gradient effects in the vicinity of grain boundary interfaces.

**Key words:** gradient plasticity, internal length scale, latent hardening, incremental energy minimization, slip systems, grain boundaries.

Copyright © 2019 by IPPT PAN, Warszawa

### 1. Introduction

IN SINGLE CRYSTAL PLASTICITY, UNDER PRESCRIBED LOADING CONDITIONS, plastic deformation is ensured by a combination of slips on the different slip systems of the crystal structure. Furthermore, plastic strain organizes in a way which makes glide the easiest, giving rise to either homogeneous or heterogeneous deformation landscapes. Slip system activity is controlled by several phenomena potentially operating at different scales and strain levels. First, for most of the crystalline structures, the number of slip systems is higher than the one necessary to accommodate any plastic strain. As a consequence, under prescribed deformation, the crystal has the possibility to select some of them in accordance with their more or less favorable orientation towards the loading direction (quantified by the Schmid factor in uniaxial stress) and with the evolution of

critical shear stresses, which leads to the extinction of some of the redundant systems. Substantially, latent hardening between the different systems influences activation in the sense that co-activation of pairs of systems with strong latent hardening, which raises their critical shear stresses significantly, does not occur if not necessary (it has been observed in single crystal experiments by KOCKS [1] and FRANCIOSI and ZAOUÏ [2] for instance).

In a second time, the segregation of the selected systems in separated zones, still preventing the coexistence of strongly interacting systems, may occur provided that a kinematically admissible heterogeneous strain pattern could be generated. Segregation has been identified for large deformations in the early works of PIERCY *et al.* [3] and SAIMOTO [4] and characterized in the shear experiments of DMITRIEVA *et al.* [5]. It was displayed in crystal plasticity simulations by various authors (in a bi-dimensional case by YALCINKAYA *et al.* [6] and for a tridimensional FCC structure by DEQUIEDT *et al.*, [7] and WANG *et al.* [8] among others).

At last, in single slip areas, plastic strain localization may arise owing to any kind of softening effect in the slip behavior (Portevin-Le Chatelier effect, Lüders bands, dislocation cell formation, ...). This was displayed in the simulations of KLUSEMANN *et al.* [9] and LANCIONI *et al.* [10] for a generic non-monotonous shear strain-shear stress curve.

From an analytical point of view, in rate-independent crystal plasticity, the plastic slip organization can be justified by energy considerations. Namely, when the elasto-plastic behavior is derived from a free energy potential (function of elastic deformation and slip fields for the different systems), a stable solution of the single crystal incremental loading problem minimizes the second order time evolution of a potential energy of the whole body. The baselines were given in NGUYEN [11] and applied to slip system activity in crystal plasticity by ORTIZ and REPETTO [12]: the approach encompasses all situations of loading or unloading among the slip systems<sup>1</sup>. For multi-slip, as has been established by PETRYK and KURSA [15], an incremental work potential does exist provided that the hardening matrix (restricted to the set of active systems) is symmetric. The ongoing selection of slip systems at a material point for various loading paths was investigated in this way by PETRYK and KURSA [16]. The formation of laminate structures of given orientations linked to system segregation is analyzed as a bifurcation of the homogeneous deformation path which is energetically favorable. The approach is developed in ORTIZ *et al.* [17] and [15] for tridimensional crystal structures and in KRATOCHVIL and KRUIK [18] for a plane double slip configuration. In the former studies, a crucial role is played by latent-to-self hardening

---

<sup>1</sup>The same kind of approach, using a potential energy for irreversible processes has been developed in damage mechanics (see for instance BOURDIN *et al.* [13] or PHAM *et al.* [14]).

ratios: the hardening matrix of PEIRCE *et al.* [19] is adopted in [15–18] in which the ratios are assumed higher than unity for both coplanar and intersecting systems. Finally, the localization pattern for single slip configurations can also be derived from an incremental energy minimum principle: it happens when the slip system free energy is non-convex: (see [10] and LANCIONI *et al.* [20] in which analytical solutions are provided for a one-dimensional problem).

It can also be assumed that slip system segregation and plastic slip localization are triggered by growing perturbation modes of the basic homogeneous deformation response. The existence of such modes is justified by a stability analysis and their time evolution is ruled by linear equations. Such relations hold as long as the constitutive behavior can be linearized in the vicinity of the basic solution which implies viscoplastic regularization of the slip system flow rules. Although this second approach only focuses on the onset of the two former processes and does not investigate fully localized solutions, the derivation of the behavior from a free energy is no longer required and the restriction to a symmetric hardening matrix can be removed. Following MOLINARI [21], plane wave (band type) perturbation modes were displayed in [7] and the laminar segregation identified by simulation was retrieved both in terms of orientation and slip systems involved: the hardening matrix was driven from the dislocation interaction coefficients identified by dislocation dynamics simulations (KUBIN *et al.* [22]) and integrated in a Teodosiu type hardening law (TEODOSIU *et al.* [23]).

However, concerning the development of heterogeneous deformation solutions, strain gradient plasticity effects are of primary importance. They introduce constitutive length scales in the single crystal models which control the size of strain heterogeneities. In case when strain localization or laminar segregation is energetically favorable, the addition of gradient terms to the free energy potential is a necessary condition for the existence of a unique solution with a finite pattern size (see [9, 10] for instance). In the stability analysis, the growth rate of plane wave perturbation modes then depends on their wavenumber which drives the band thickness and spacing (DEQUIEDT [24]). For a number of constitutive models, it is assumed that non-local effects arise from the storage of polar dislocations under slip rate gradients: they generate microforces which modify the effective resolved shear stress (the additional term is referred to as the “back stress”) and induce kinematic hardening in the slip system flow rules (YEFIMOV *et al.* [25], EVERS *et al.* [26], BAYLEY *et al.* [27], KURODA and TVERGAARD [28])<sup>2</sup>. Several authors (GURTIN [34], ERTURK *et al.* [35]) derived micro-forces from a so-called

---

<sup>2</sup>In a couple of works, polar dislocations densities also act as additional densities in the hardening law (see FLECK *et al.* [29], GAO *et al.* [30], EVERS *et al.* [31], MA *et al.* [32], PETRYK and STUPKIEWICZ [33], among others); in the present work, this effect is disregarded.

defect energy expressing as a convex potential of polar dislocation densities or, equivalently, of slip gradients. In this case, the non-local effects can be incorporated in a variational approach.

Furthermore, the equilibrium of microforces on a single crystal volume of finite size requires additional boundary conditions either on microforces themselves or on plastic slips (see GURTIN and NEEDLEMAN [36] or [35]). A common assumption is the one of micro-hard (or micro-clamped) conditions which amount to a null polar dislocation flow through the boundary [36]. They are representative of the behavior of grain boundary interfaces, at least as a first order approximation, since the latter are supposed not to be crossed by mobile dislocations because of the incompatibility of the two crystal lattices. In most cases, such conditions lead to non-uniform deformation profiles confining plastic strain in the bulk and concentrating dislocation densities in a limit layer near the boundary. This has been illustrated by various authors in the one-dimensional framework of a strip in simple shear subject to plane double slip (EVERS *et al.* [31], YEFIMOV and VAN DER GIESSEN [37]); the slip rate profiles depend primarily on the ratio between the strip thickness and the constitutive length scale of the gradient model. The incidence of micro-hard boundary conditions on band localization and laminar segregation has also been evaluated in bi-dimensional simulations [9]: the laminar structure, which is usually not parallel to the boundary, is preserved in the bulk as long as the length scale of the model, which drives the extent of the limit layer, is much lower than the specimen size.

In case of slip system redundancy, the coupling of strain gradient plasticity with micro-hard boundary conditions influences system selection in the neighborhood of interfaces (independently of strain compatibility concerns at the scale of the aggregate). Whereas inside grains, the selection is an outcome of system orientation and self and latent hardening essentially, in the limit layer, non-local effects and the way they couple the slip rate gradients on the different systems ought to control system activation. This question can be addressed by applying the energy minimizing approach of [16] to a finite volume including the boundary. In this purpose, the former one-dimensional strip problem is here extended to cases with three coplanar slip systems (two being sufficient to accommodate any isochoric plastic strain under plane strain conditions). The respective influence of the slip system orientations, the latent hardening coefficients and the length scale of non-local effects is investigated. Two gradient rate-independent plasticity theories, developed by Gurtin and co-workers, are considered. In the first one, the free energy is proportional to the sum of square of polar dislocation densities (see, GURTIN *et al.* [38]) and yields, for each slip system, a back stress linear in the second derivative of slip for the system itself (an equivalent assumption is made in [6] and [9]). In the second one, the free energy and therefore back

stresses are functions of a dislocation density tensor [21], coupling the different slip gradients. Among the three systems, a low latent hardening modulus is assumed for at least two of them: therefore, single slip segregation and an oriented laminar structure is unlikely to occur, which validates one-dimensional solutions.

The single crystal constitutive relations are presented in Section 2.1 and the variational formulation of a time evolution problem is achieved for the two models. It is particularized to the one-dimensional strip case in Section 2.2. For three potentially active slip systems, the profile in the band thickness of the different slip rates and mechanical variables are displayed in Section 3: the areas of activation of the different systems are analyzed in terms of energy minimization. The influence of the slip system orientations, latent hardening moduli and the intensity of gradient effects are investigated; the difference between the two gradient theories is also emphasized.

## 2. Framework

### 2.1. Gradient plasticity model and formulation of the boundary value problem

In this study, quasi-static loading (equilibrium) is considered and a small deformation elasto-plastic formalism is retained. It yields an additive decomposition of the displacement gradient into an elastic and a plastic part:

$$(2.1) \quad \mathbf{U} = \text{grad}(\mathbf{u}) = \mathbf{U}^e + \mathbf{U}^p.$$

The elastic transformation can be split into its symmetric (deformation) and skew-symmetric (rotation) parts and the elastic-plastic decomposition is such that  $\boldsymbol{\omega}^e$  is the rotation of the crystal lattice:

$$(2.2) \quad \mathbf{U}^e = \boldsymbol{\varepsilon}^e + \boldsymbol{\omega}^e.$$

The plastic transformation is given by summing plastic slip over all slip systems  $\alpha$  ( $\mathbf{n}^\alpha$  is the slip plane normal and  $\mathbf{m}^\alpha$  the slip direction):

$$(2.3) \quad \mathbf{U}^p = \sum_{\alpha} \gamma^{\alpha} \mathbf{m}^{\alpha} \otimes \mathbf{n}^{\alpha}.$$

The total deformation reads:

$$(2.4) \quad \boldsymbol{\varepsilon} = \boldsymbol{\varepsilon}^e + \boldsymbol{\varepsilon}^p \quad \text{with} \quad \boldsymbol{\varepsilon}^p = \sum_{\alpha} \frac{\gamma^{\alpha}}{2} (\mathbf{m}^{\alpha} \otimes \mathbf{n}^{\alpha} + \mathbf{n}^{\alpha} \otimes \mathbf{m}^{\alpha}).$$

In this work, slip systems are supposed to be activated always in the same sense and  $\mathbf{m}^\alpha$  denotes oriented slip directions; therefore  $\gamma^\alpha \geq 0$ .

Plastic transformation gradients result in the accumulation of polar dislocation densities (usually called geometrically necessary dislocation (GND) densities). A measure of GND densities is given by a dislocation density tensor introduced by NYE [39] which quantifies the non-closure of Burgers circuits induced by plastic deformation (see CERMELLI and GURTIN [40]):

$$(2.5) \quad \mathbf{G} = \text{curl}(\mathbf{U}^p)^3.$$

$\text{curl}(\mathbf{U}^p)$  also reads as a function of slip gradients (using Eq. (2.3)):

$$(2.6) \quad \text{curl}(\mathbf{U}^p) = \sum_{\alpha} \mathbf{m}^{\alpha} \otimes (\text{grad}(\gamma^{\alpha}) \times \mathbf{n}^{\alpha}).$$

On the other hand, the dislocation density tensor is a function of the edge and screw components  $\rho_e^{\alpha}$  and  $\rho_s^{\alpha}$  of the polar densities of each slip system (following ARSENLIS and PARKS [41]):

$$(2.7) \quad \mathbf{G} = \sum_{\alpha} b(\rho_e^{\alpha} \mathbf{m}^{\alpha} \otimes \mathbf{p}^{\alpha} + \rho_s^{\alpha} \mathbf{m}^{\alpha} \otimes \mathbf{m}^{\alpha}),$$

with  $b$  the Burgers vector and  $\mathbf{p}^{\alpha} = \mathbf{n}^{\alpha} \times \mathbf{m}^{\alpha}$ .

Assuming that accommodation of plastic strain gradients operates slip system by slip system and owing to Eqs. (2.6) and (2.7), edge and screw densities are related to slip rate gradients in the following way [38]:

$$(2.8) \quad b\rho_e^{\alpha} = -\text{grad}(\gamma^{\alpha}) \cdot \mathbf{m}^{\alpha} \quad \text{and} \quad b\rho_s^{\alpha} = \text{grad}(\gamma^{\alpha}) \cdot \mathbf{p}^{\alpha}.$$

Micro-forces can be derived by postulating the existence of a free energy  $\Psi$  function of polar dislocation densities (defect energy). From a physical point of view, one possible origin of defect energy is the interaction forces between individual dislocations (i.e. depending on the interaction of their elastic fields)<sup>4</sup>. At the scale of continuum, it is linked to spatial correlation in the dislocation distribution function (the transition from discrete to continuum is beyond the scope of the present paper but the interested reader is referred to GROMA *et al.* [43] for instance). In a first class of models (called *M1 models* in the following),  $\Psi$  is a positive definite bilinear form of the edge and screw densities per systems [38]<sup>5</sup>.

<sup>3</sup>The curl of a second order tensor  $\mathbf{A}$  and its cross product with a first order tensor  $\mathbf{b}$  are defined respectively by  $(\text{curl}(\mathbf{A}))_{ij} = \mathbf{e}_{jlk} A_{ik,l}$  and  $(\mathbf{A} \times \mathbf{b})_{ij} = \mathbf{e}_{jlk} A_{il} b_k$  ( $\mathbf{e}_{jlk}$  is the Levi-Civita permutation symbol); the notation  $(\mathbf{A} \times)$ , introduced in [36] denotes the third order tensor of components  $(\mathbf{A} \times)_{ijk} = \mathbf{e}_{jlk} A_{il}$ . Let us notice that, as  $\mathbf{U}$  is a gradient, equivalently,  $\mathbf{G} = -\text{curl}(\mathbf{U}^e)$ .

<sup>4</sup>In some works, the defect energy is associated with the self-energy of GND (OHNO and OKUMURA [42]), but this assumption is not considered here.

<sup>5</sup>In [38], dissipative micro-forces are added to the ones driven from the defect energy but they are neglected in the present work.

In a second class of models (called *M2 models* in the following), it is assumed that  $\Psi$  is quadratic in the dislocation density tensor [34] (which integrates the effect of polar densities globally). The two cases are investigated in this work: some comments about the physical meaning of the two defect energies are provided in the conclusion.

Let us notice that the time evolutions of  $\mathbf{G}$ ,  $\rho_e^\alpha$  and  $\rho_s^\alpha$ , derived from Eqs. (2.5) and (2.8) respectively, also express as balance equations (superimposed dot is for time derivatives):

$$(2.9) \quad \dot{\mathbf{G}} = -\operatorname{div}(\dot{\mathbf{U}}^p \times), \quad b\dot{\rho}_e^\alpha = -\operatorname{div}(\dot{\gamma}^\alpha \mathbf{m}^\alpha) \quad \text{and} \quad b\dot{\rho}_s^\alpha = -\operatorname{div}(-\dot{\gamma}^\alpha \mathbf{p}^\alpha),$$

in which  $(\dot{\mathbf{U}}^p \times)$  is the dislocation tensor flux and  $\dot{\gamma}^\alpha \mathbf{m}^\alpha$  and  $-\dot{\gamma}^\alpha \mathbf{p}^\alpha$  are edge and screw dislocation fluxes [36].

On a material volume  $\Omega$ , macroscopic equilibrium and plastic flow conditions are derived from an extended principle of virtual power in which virtual material velocity  $\hat{\mathbf{v}}$  and shearing rates  $\hat{\gamma}^\alpha$  are specified independently [34]. The virtual power of external forces writes, in the absence of body forces, as a linear form of surface traction  $\mathbf{t}$  on the boundary  $\partial\Omega$ :

$$(2.10) \quad P_{\text{ext}}(\hat{\mathbf{v}}) = \int_{\partial\Omega} \mathbf{t} \cdot \hat{\mathbf{v}} da.$$

The virtual power of internal forces is expended by Cauchy stress conjugate to elastic strain rate, critical shear stresses conjugate to slip rates and micro-forces conjugate to slip rate gradients. The power expenditure of micro-forces balances the increase of the defect energy. Therefore, owing Eq. (2.8), for the *M1 models*, they expend power over slip rate gradients and more precisely over the slip plane components of these gradients:

$$(2.11) \quad P_{\text{int}}(\hat{\mathbf{v}}, \hat{\gamma}^\alpha) = - \int_{\Omega} \boldsymbol{\sigma} : \hat{\boldsymbol{\varepsilon}}^e d\Omega - \sum_{\alpha} \int_{\Omega} (\tau_c^\alpha \hat{\gamma}^\alpha + \boldsymbol{\xi}^\alpha \cdot \operatorname{grad}^\alpha(\hat{\gamma}^\alpha)) d\Omega,$$

with

$$\operatorname{grad}^\alpha(\hat{\gamma}^\alpha) = (\operatorname{grad}(\hat{\gamma}^\alpha) \cdot \mathbf{m}^\alpha) \mathbf{m}^\alpha + (\operatorname{grad}(\hat{\gamma}^\alpha) \cdot \mathbf{p}^\alpha) \mathbf{p}^\alpha.$$

For *M2 models*, owing (2.5), the virtual power of internal forces is expended by a micro-force conjugate to  $\operatorname{curl}(\dot{\mathbf{U}}^p)$  since non-local effects are correlated with the evolution of the dislocation density tensor  $\mathbf{G}$ :

$$(2.12) \quad P_{\text{int}}(\hat{\mathbf{v}}, \hat{\gamma}^\alpha) = - \int_{\Omega} \boldsymbol{\sigma} : \hat{\boldsymbol{\varepsilon}}^e d\Omega - \sum_{\alpha} \int_{\Omega} \tau_c^\alpha \hat{\gamma}^\alpha d\Omega - \int_{\Omega} \mathbf{T} : \operatorname{curl}(\dot{\mathbf{U}}^p) d\Omega.$$

Let us assume, as classically, that material velocity is prescribed on one part of the boundary and surface traction is prescribed on the complement:

$$(2.13) \quad \mathbf{v} = \mathbf{v}^d \quad \text{on } \partial\Omega_u \quad \text{and} \quad \mathbf{t} = \mathbf{t}^d \quad \text{on } \partial\Omega_\sigma = \partial\Omega \setminus \partial\Omega_u.$$

In case of micro-hard conditions on  $\partial\Omega$ , for *M1 models*, it is natural to assume that screw and edge dislocation density flows are prohibited, namely shearing rates annihilate for all slip planes intersecting  $\partial\Omega$  ( $\mathbf{n}$  is the outward unit normal to  $\partial\Omega$ ):

$$(2.14) \quad \dot{\gamma}^\alpha \mathbf{m}^\alpha \cdot \mathbf{n} = \dot{\gamma}^\alpha \mathbf{p}^\alpha \cdot \mathbf{n} = \mathbf{0} \quad \text{on } \partial\Omega.$$

For *M2 models*, it is natural to assume that the dislocation density tensor flow is prohibited:

$$(2.15) \quad \dot{\mathbf{U}}^p \times \mathbf{n} = \mathbf{0} \quad \text{on } \partial\Omega.$$

The condition (2.15) is weaker than the condition (2.14) and, as we shall see in Section 3, can be fulfilled for some combinations of non-zero shearing rates<sup>6</sup>:

Due to Eqs. (2.14) and (2.15), integration by parts of Eqs. (2.11) and (2.12) yield for *M1 models* and *M2 models* respectively ( $\tau^\alpha = \boldsymbol{\sigma} : (\mathbf{m}^\alpha \otimes \mathbf{n}^\alpha)$  is the resolved shear stress):

$$(2.16) \quad P_{int}(\hat{\mathbf{v}}, \hat{\gamma}^\alpha) = \int_{\Omega} \operatorname{div}(\boldsymbol{\sigma}) \cdot \hat{\mathbf{v}} d\Omega - \int_{\partial\Omega} (\boldsymbol{\sigma} \cdot \mathbf{n}) \cdot \hat{\mathbf{v}} da \\ + \sum_{\alpha} \int_{\Omega} (\tau^\alpha - \tau_c^\alpha + \operatorname{div}(\boldsymbol{\xi}^\alpha)) \hat{\gamma}^\alpha d\Omega,$$

$$(2.17) \quad P_{int}(\hat{\mathbf{v}}, \hat{\gamma}^\alpha) = \int_{\Omega} \operatorname{div}(\boldsymbol{\sigma}) \cdot \hat{\mathbf{v}} d\Omega - \int_{\partial\Omega} (\boldsymbol{\sigma} \cdot \mathbf{n}) \cdot \hat{\mathbf{v}} da \\ + \sum_{\alpha} \int_{\Omega} (\tau^\alpha - \tau_c^\alpha - \operatorname{curl}(\mathbf{T}) : (\mathbf{m}^\alpha \otimes \mathbf{n}^\alpha)) \hat{\gamma}^\alpha d\Omega.$$

In Gurtin and co-workers [29–31], equilibrium holds when the power of all forces annihilates for any virtual fields  $\hat{\mathbf{v}}$  and  $\hat{\gamma}^\alpha \geq 0$  satisfying boundary conditions Eqs. (2.13)<sub>1</sub> and (2.14) or (2.15):

$$(2.18) \quad P_{ext}(\hat{\mathbf{v}}) + P_{int}(\hat{\mathbf{v}}, \hat{\gamma}^\alpha) = 0,$$

<sup>6</sup>Indeed, it is also proved in [36] that the condition (2.15) is the one which guarantee the well-posedness of a boundary value problem with a M2 type defect energy.

and, as it holds for the actual fields  $\mathbf{v}$  and  $\dot{\gamma}^\alpha$ :

$$(2.19) \quad P_{ext}(\mathbf{v} - \hat{\mathbf{v}}) + P_{int}(\mathbf{v} - \hat{\mathbf{v}}, \dot{\gamma}^\alpha - \hat{\dot{\gamma}}^\alpha) = 0.$$

This generalized principle of virtual power implies, apart from the equilibrium of macroscopic forces in the bulk and on the boundary, the micro-force balance equations in which non-local effects provide, for each slip system, a so-called “back stress”  $\tau_b^\alpha$  in the yield function (left-hand side of equality):

$$(2.20) \quad \tau^\alpha - (\tau_c^\alpha + \tau_b^\alpha) = 0 \quad \text{in } \Omega,$$

with  $\tau_b^\alpha = -\text{div}(\boldsymbol{\xi}^\alpha)$  for *M1 models* and  $\tau_b^\alpha = \text{curl}(\mathbf{T}) : (\mathbf{m}^\alpha \otimes \mathbf{n}^\alpha)$  for *M2 models*.

Still, in rate-independent plasticity (with oriented slip systems), critical shear stresses act as thresholds; plastic slip cannot decrease and annihilates whenever the yield function is strictly negative. Namely, micro-force balance reads:

$$(2.21) \quad (\tau^\alpha - (\tau_c^\alpha + \tau_b^\alpha)) \leq 0, \quad \dot{\gamma}^\alpha \geq 0 \quad \text{and} \quad (\tau^\alpha - (\tau_c^\alpha + \tau_b^\alpha))\dot{\gamma}^\alpha = 0.$$

Equivalently, the plastic slip rate maximizes plastic work in the sense that:

$$(2.22) \quad \dot{\gamma}^\alpha \geq 0 \quad \text{and} \quad (\tau^\alpha - (\tau_c^\alpha + \tau_b^\alpha))(\dot{\gamma}^\alpha - \hat{\dot{\gamma}}^\alpha) \geq 0 \quad \text{for all } \hat{\dot{\gamma}}^\alpha \geq 0.$$

The virtual power principle then writes in the following way (Eq. (2.19) holds when the yield function is zero for all slip systems):

$$(2.23) \quad P_{ext}(\mathbf{v} - \hat{\mathbf{v}}) + P_{int}(\mathbf{v} - \hat{\mathbf{v}}, \dot{\gamma}^\alpha - \hat{\dot{\gamma}}^\alpha) \geq 0,$$

for all fields  $\hat{\mathbf{v}}$  and  $\hat{\dot{\gamma}}^\alpha \geq 0$ .

Let us now assume that elasticity is linear and that critical shear stresses are linear functions of plastic slips, the hardening matrix being symmetric:

$$(2.24) \quad \boldsymbol{\sigma} = \mathbb{C} : \boldsymbol{\varepsilon}^e \quad \text{and} \quad \tau_c^\alpha = H_{\alpha\beta}\gamma^\beta \quad \text{with} \quad H_{\beta\alpha} = H_{\alpha\beta}.$$

The defect energy  $\Psi$  is a function of polar dislocation densities  $\Psi(\rho_e^\alpha, \rho_s^\alpha)$  for *M1 models* [38] and microforces are assumed non-dissipative; therefore:

$$(2.25) \quad \sum_{\alpha} \boldsymbol{\xi}^\alpha \cdot \text{grad}^\alpha(\dot{\gamma}^\alpha) = \dot{\Psi} = \sum_{\alpha} \left( \frac{\partial \Psi}{\partial \rho_e^\alpha} \dot{\rho}_e^\alpha + \frac{\partial \Psi}{\partial \rho_s^\alpha} \dot{\rho}_s^\alpha \right).$$

Owing to Eq. (2.8):

$$(2.26) \quad \boldsymbol{\xi}^\alpha = \frac{1}{b} \left( -\frac{\partial \Psi}{\partial \rho_e^\alpha} \mathbf{m}^\alpha + \frac{\partial \Psi}{\partial \rho_s^\alpha} \mathbf{p}^\alpha \right).$$

The defect energy  $\Psi$  is a function of the dislocation density tensor  $\mathbf{G}$  for *M2 models*:

$$(2.27) \quad \mathbf{T} : \text{curl}(\dot{\mathbf{U}}^p) = \dot{\Psi} = \frac{d\Psi}{d\mathbf{G}} : \dot{\mathbf{G}} \quad \text{and, therefore: } \mathbf{T} = \frac{d\Psi}{d\mathbf{G}}.$$

In both cases, by virtue of Eqs. (2.8) and (2.6),  $\Psi$  expresses as a function of slip gradients and equilibrium relations may be re-formulated using a potential energy  $E(\mathbf{u}, \gamma^\alpha, \mathbf{t}^d)$  of material displacement, plastic slip fields and loading parameter  $\mathbf{t}^d$ . Eqs. (2.19) and (2.23) give respectively:

$$(2.28) \quad \begin{aligned} E_{,\mathbf{u}} \cdot (\mathbf{v} - \hat{\mathbf{v}}) + \sum_{\alpha} E_{,\gamma^\alpha} \cdot (\dot{\gamma}^\alpha - \hat{\dot{\gamma}}^\alpha) &= 0, \\ E_{,\mathbf{u}} \cdot (\mathbf{v} - \hat{\mathbf{v}}) + \sum_{\alpha} E_{,\gamma^\alpha} \cdot (\dot{\gamma}^\alpha - \hat{\dot{\gamma}}^\alpha) &\geq 0, \end{aligned}$$

with:

$$(2.29) \quad \begin{aligned} E(\mathbf{u}, \gamma^\alpha, \mathbf{t}^d) &= \int_{\Omega} \left( \frac{1}{2} (\boldsymbol{\varepsilon} - \boldsymbol{\varepsilon}^p) : \mathbb{C} : (\boldsymbol{\varepsilon} - \boldsymbol{\varepsilon}^p) + \sum_{\alpha, \beta} \frac{1}{2} \gamma^\alpha H_{\alpha\beta} \gamma^\beta + \Psi \right) d\Omega \\ &\quad - \int_{\partial\Omega_\sigma} (\mathbf{t}^d \cdot \mathbf{u}) da. \end{aligned}$$

Following the notations of [11], in Eq. (2.28),  $E_{,\mathbf{u}} \cdot \delta\mathbf{u}$  and  $E_{,\gamma^\alpha} \cdot \delta\gamma^\alpha$  hold for the first variations of  $E$  with respects to  $\mathbf{u}$  and  $\gamma^\alpha$ ; for instance:

$$(2.30) \quad E_{,\mathbf{u}} \cdot \delta\mathbf{u} = \int_{\Omega} (\mathbb{C} : (\boldsymbol{\varepsilon} - \boldsymbol{\varepsilon}^p)) : \delta\boldsymbol{\varepsilon} d\Omega - \int_{\partial\Omega_\sigma} (\mathbf{t}^d \cdot \delta\mathbf{u}) da.$$

At a time  $t$ , let us restrict the set of slip systems to the ones for which the yield function is zero. Equilibrium relations written at times  $t$  and  $t + dt$  yield:

$$(2.31) \quad \begin{aligned} E_{,\mathbf{u}} \cdot (\dot{\mathbf{v}} - \hat{\dot{\mathbf{v}}}) + \sum_{\alpha} E_{,\gamma^\alpha} \cdot (\ddot{\gamma}^\alpha - \hat{\ddot{\gamma}}^\alpha) \\ + \left( \dot{\mathbf{t}}^d \cdot E_{,\mathbf{t}^d \mathbf{u}} + \mathbf{v} \cdot E_{,\mathbf{u}\mathbf{u}} + \sum_{\beta} \dot{\gamma}^\beta \cdot E_{,\gamma^\beta \mathbf{u}} \right) \cdot (\mathbf{v} - \hat{\mathbf{v}}) \\ + \sum_{\alpha} \left( \mathbf{v} \cdot E_{,\gamma^\alpha \mathbf{u}} + \sum_{\beta} \dot{\gamma}^\beta \cdot E_{,\gamma^\alpha \gamma^\beta} \right) (\dot{\gamma}^\alpha - \hat{\dot{\gamma}}^\alpha) \geq 0. \end{aligned}$$

In Eq. (2.31),  $\delta\tilde{\mathbf{u}} \cdot E_{,\mathbf{u}\mathbf{u}} \cdot \delta\mathbf{u}$ ,  $\delta\tilde{\mathbf{u}} \cdot E_{,\mathbf{u}\gamma^\alpha} \cdot \delta\gamma^\alpha$ , ... hold for the second variations of  $E$ ; namely:

$$(2.32) \quad \delta\tilde{\mathbf{u}} \cdot E_{,\mathbf{u}\mathbf{u}} \cdot \delta\mathbf{u} = \int_{\Omega} \delta\tilde{\boldsymbol{\varepsilon}} : \mathbb{C} : \delta\boldsymbol{\varepsilon} d\Omega.$$

Owing to Eq. (2.28)<sub>1</sub>:

$$(2.33) \quad E_{,\mathbf{u}} \cdot (\dot{\mathbf{v}} - \hat{\mathbf{v}}) + \sum_{\alpha} E_{,\dot{\gamma}^{\alpha}} \cdot (\ddot{\gamma}^{\alpha} - \hat{\dot{\gamma}}^{\alpha}) = 0.$$

Therefore, every solution  $(\mathbf{v}, \dot{\gamma}^{\alpha})$  of the system evolution is given by the following relation:

$$(2.34) \quad \left( \dot{\mathbf{t}}^d \cdot E_{,\mathbf{t}^d \mathbf{u}} + \mathbf{v} \cdot E_{,\mathbf{u}\mathbf{u}} + \sum_{\beta} \dot{\gamma}^{\beta} \cdot E_{,\dot{\gamma}^{\beta} \mathbf{u}} \right) \cdot (\mathbf{v} - \hat{\mathbf{v}}) \\ + \sum_{\alpha} \left( \mathbf{v} \cdot E_{,\dot{\gamma}^{\alpha} \mathbf{u}} + \sum_{\beta} \dot{\gamma}^{\beta} \cdot E_{,\dot{\gamma}^{\alpha} \dot{\gamma}^{\beta}} \right) (\dot{\gamma}^{\alpha} - \hat{\dot{\gamma}}^{\alpha}) \geq 0.$$

A sufficient condition for  $(\mathbf{v}, \dot{\gamma}^{\alpha})$  to fulfill Eq. (2.34) is to minimize the quadratic pseudo-potential:

$$(2.35) \quad J(\hat{\mathbf{v}}, \hat{\dot{\gamma}}^{\alpha}) = \dot{\mathbf{t}}^d \cdot E_{,\mathbf{u}\mathbf{t}^d} \cdot \hat{\mathbf{v}} + \frac{1}{2} \hat{\mathbf{v}} \cdot E_{,\mathbf{u}\mathbf{u}} \cdot \hat{\mathbf{v}} \\ + \sum_{\alpha} \hat{\mathbf{v}} \cdot E_{,\mathbf{u}\dot{\gamma}^{\alpha}} \cdot \hat{\dot{\gamma}}^{\alpha} + \frac{1}{2} \sum_{\alpha, \beta} \hat{\dot{\gamma}}^{\alpha} \cdot E_{,\dot{\gamma}^{\alpha} \dot{\gamma}^{\beta}} \cdot \hat{\dot{\gamma}}^{\beta}.$$

Among solutions of Eq. (2.34), the one satisfying Eq. (2.35) is stable in the sense that it leads to a minimum of the potential energy at time  $t + dt$  for a given state at time  $t$  (owing to that  $E$  is assimilated to its second order development in  $dt$  [16]).

## 2.2. Bi-dimensional framework

Let us now consider the classical bi-dimensional problem of a band of thickness  $h$  under shear deformation (Fig. 1). All mechanical quantities depend on the  $y$  coordinate and material displacement in the  $z$  direction is zero (in what follows,  $\mathbf{e}_x$ ,  $\mathbf{e}_y$  and  $\mathbf{e}_z$  are unit vectors in the  $x$ ,  $y$  and  $z$  direction respectively):

$$(2.36) \quad \mathbf{u} = u_x(y)\mathbf{e}_x + u_y(y)\mathbf{e}_y.$$

Boundary conditions are of imposed displacement:

$$(2.37) \quad u_x(y=0) = 0, \quad u_x(y=h) = U \quad \text{and} \quad u_y(y=0, h) = 0.$$

Slip systems have their slip plane normal and slip directions in the  $(x,y)$  plane and dislocations are of edge type with dislocation lines collinear to the  $z$ -axis. The elastic behavior is supposed to be isotropic ( $\lambda$  and  $\mu$  are the Lamé and shear moduli):

$$(2.38) \quad \boldsymbol{\varepsilon}^e : \mathbb{C} : \boldsymbol{\varepsilon}^e = \lambda(\text{Tr}(\boldsymbol{\varepsilon}^e))^2 + 2\mu(\boldsymbol{\varepsilon}^e : \boldsymbol{\varepsilon}^e).$$

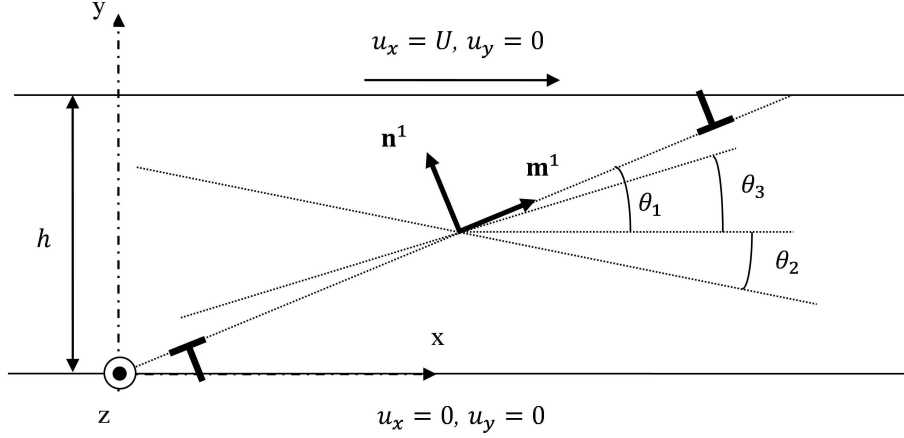


FIG. 1. Geometry, loading conditions and orientations of the three slip systems for the band.

Self-hardening moduli are set equal and latent to self hardening ratios  $q_{\alpha\beta}$  are defined for all pairs of systems:

$$(2.39) \quad H_{\alpha\alpha} = H \quad \text{and} \quad H_{\alpha\beta} = q_{\alpha\beta}H.$$

A *M1 model* with defect energy quadratic in edge densities [38] and a *M2 model* with defect energy quadratic in the norm of tensor  $\mathbf{G}$  [34] are considered in the following:

$$(2.40) \quad \begin{aligned} \Psi_1(\rho_e^\alpha) &= \frac{1}{2}S_0L^2b^2 \sum_{\alpha} \rho_e^{\alpha^2}, \\ \Psi_2(\mathbf{G}) &= \frac{1}{2}S_0L^2\|\mathbf{G}\|^2 \end{aligned} \quad \text{with} \quad \|\mathbf{G}\|^2 = \mathbf{G} : \mathbf{G}.$$

It is clear from Eq. (2.29) that  $S_0$  has dimension of stress and it can be set equal to twice the shear modulus ( $S_0 = 2\mu$ ) without loss of generality, the intensity of non-local effects being captured by the characteristic length  $L$ . Let us observe that  $\Psi_1$  assumes no coupling between polar dislocations of the different systems.

The edge densities and the dislocation density tensor are given respectively by:

$$(2.41) \quad b\rho_e^\alpha = -\frac{d\gamma^\alpha}{dy}(\mathbf{m}^\alpha \cdot \mathbf{e}_y) \quad \text{and} \quad \mathbf{G} = -\sum_{\alpha} \frac{d\gamma^\alpha}{dy}(\mathbf{n}^\alpha \cdot \mathbf{e}_x)\mathbf{m}^\alpha \otimes \mathbf{e}_z.$$

For the two models, micro-hard boundary conditions given by Eqs. (2.14) and (2.15) yield:

$$(2.42) \quad \dot{\gamma}^\alpha(y=0, h)(\mathbf{m}^\alpha \cdot \mathbf{e}_y) = 0$$

and

$$\dot{\mathbf{U}}^p(y=0, h) \times \mathbf{e}_y = \sum_{\alpha} \dot{\gamma}^{\alpha}(y=0, h) (\mathbf{n}^{\alpha} \cdot \mathbf{e}_x) \mathbf{m}^{\alpha} \otimes \mathbf{e}_z = \mathbf{0}.$$

After some straightforward calculations, the pseudo-potential, defined for a unit length in the  $x$  direction and unit thickness in the  $z$  direction, expresses in non-dimensional form as the sum of a local and a non-local component:

$$(2.43) \quad J(\hat{\mathbf{v}}, \hat{\gamma}^{\alpha}) = \frac{2\mu\dot{U}^2}{h} (\bar{J}_{loc}(\bar{\mathbf{v}}, \bar{\gamma}^{\alpha}) + \bar{J}_{non\_loc}(\bar{\mathbf{v}}, \bar{\gamma}^{\alpha})),$$

with  $(\{\mathbf{A}\}_S$  is for the symmetric part of tensor  $\mathbf{A}$ ):

$$(2.44) \quad \begin{aligned} \bar{J}_{loc}(\bar{\mathbf{v}}, \bar{\gamma}^{\alpha}) = & \frac{1}{2} \int_0^1 \left( (\bar{\lambda} + 1) \left( \frac{d\bar{v}_y}{d\bar{y}} \right)^2 + \frac{1}{2} \left( \frac{d\bar{v}_x}{d\bar{y}} \right)^2 \right. \\ & - 2 \left( \frac{d\bar{v}_x}{d\bar{y}} \right) \sum_{\alpha} \bar{\gamma}^{\alpha} (\mathbf{e}_x \cdot \{\mathbf{m}^{\alpha} \otimes \mathbf{n}^{\alpha}\}_S \cdot \mathbf{e}_y) \\ & - 2 \left( \frac{d\bar{v}_y}{d\bar{y}} \right) \sum_{\alpha} \bar{\gamma}^{\alpha} (\mathbf{e}_y \cdot \{\mathbf{m}^{\alpha} \otimes \mathbf{n}^{\alpha}\}_S \cdot \mathbf{e}_y) \\ & \left. + \sum_{\alpha, \beta} \bar{\gamma}^{\alpha} \bar{\gamma}^{\beta} (q_{\alpha\beta} \bar{H} + \{\mathbf{m}^{\alpha} \otimes \mathbf{n}^{\alpha}\}_S : \{\mathbf{m}^{\beta} \otimes \mathbf{n}^{\beta}\}_S) \right) d\bar{y}. \end{aligned}$$

For the *M1 model* and *M2 model*, the non-local components read respectively:

$$(2.45) \quad \begin{aligned} \bar{J}_{non\_loc.1}(\bar{\gamma}^{\alpha}) &= \frac{1}{2} \bar{L}^2 \sum_{\alpha} \int_0^1 \left( \frac{d\bar{\gamma}^{\alpha}}{d\bar{y}} \right)^2 (\mathbf{m}^{\alpha} \cdot \mathbf{e}_y)^2 d\bar{y} \\ &= \frac{1}{2} \bar{L}^2 \sum_{\alpha} \int_0^1 \left( \frac{d\bar{\gamma}^{\alpha}}{d\bar{y}} \right)^2 (\mathbf{n}^{\alpha} \cdot \mathbf{e}_x)^2 d\bar{y}, \\ \bar{J}_{non\_loc.2}(\bar{\gamma}^{\alpha}) &= \frac{1}{2} \bar{L}^2 \sum_{\alpha, \beta} \int_0^1 \left( \frac{d\bar{\gamma}^{\alpha}}{d\bar{y}} \right) \left( \frac{d\bar{\gamma}^{\beta}}{d\bar{y}} \right) \\ &\quad \times (\mathbf{n}^{\alpha} \cdot \mathbf{e}_x) (\mathbf{m}^{\alpha} \cdot \mathbf{m}^{\beta}) (\mathbf{n}^{\beta} \cdot \mathbf{e}_x) d\bar{y}. \end{aligned}$$

In the above relations, lengths are adimensioned by the band thickness, velocities by the imposed velocity  $\dot{U}$ , slip rates by the average shear strain rate and all moduli by twice the shear modulus:

$$\begin{aligned} y &= h\bar{y}, \quad L = h\bar{L}, \quad \hat{v}_x = \dot{U}\bar{v}_x, \quad \hat{v}_y = \dot{U}\bar{v}_y, \\ \hat{\gamma}^{\alpha} &= \dot{U}\bar{\gamma}^{\alpha}/h, \quad \lambda = 2\mu\bar{\lambda} \quad \text{and} \quad H = 2\mu\bar{H}. \end{aligned}$$

The time evolution of the dislocation densities and the dislocation density tensor are adimensioned as follows:

$$(2.46) \quad \begin{aligned} \bar{\rho}_e^\alpha &= \frac{h^2}{\dot{U}} (b\dot{\rho}_e^\alpha) = -\frac{d\bar{\gamma}^\alpha}{d\bar{y}} (\mathbf{m}^\alpha \cdot \mathbf{e}_y), \\ \bar{\mathbf{G}} &= \frac{h^2}{\dot{U}} \dot{\mathbf{G}} = -\sum_\alpha \frac{d\bar{\gamma}^\alpha}{d\bar{y}} (\mathbf{n}^\alpha \cdot \mathbf{e}_x) \mathbf{m}^\alpha \otimes \mathbf{e}_z. \end{aligned}$$

The time rates of the resolved shear stresses still express in non-dimensional form:

$$(2.47) \quad \dot{\tau}^\alpha = 2\mu\dot{U} \bar{\tau}^\alpha / h.$$

Time rates of the critical shear stresses are adimensioned in the same way and satisfy the following relation:

$$(2.48) \quad \bar{\tau}_c^\alpha = \bar{H}_{\alpha\beta} \bar{\gamma}^\beta.$$

Time rates of back stresses satisfy, for the *M1 model* and *M2 model* respectively:

$$(2.49) \quad \begin{aligned} \bar{\tau}_b^\alpha &= -\bar{L}^2 \left( \frac{d^2 \bar{\gamma}^\alpha}{d\bar{y}^2} (\mathbf{m}^\alpha \cdot \mathbf{e}_y)^2 \right), \\ \bar{\tau}_b^\alpha &= -\bar{L}^2 \left( \sum_\beta \left( \frac{d^2 \bar{\gamma}^\beta}{d\bar{y}^2} \right) (\mathbf{n}^\alpha \cdot \mathbf{e}_x) (\mathbf{m}^\alpha \cdot \mathbf{m}^\beta) (\mathbf{n}^\beta \cdot \mathbf{e}_x) \right). \end{aligned}$$

Below, for the sake of simplicity, non-dimensional actual and virtual fields are denoted in the same way.

Let us observe that, since  $\bar{\Psi}_1(\rho_e^\alpha)$  assumes no coupling between the dislocation densities of the different systems, no coupling emerges between slip gradients in  $\bar{J}_{non\_loc\_1}$ . On the contrary,  $\bar{\mathbf{G}}$  combines the densities on the different systems and  $\bar{J}_{non\_loc\_2}$  contains  $\alpha\beta$ -terms coupling their slip gradients (the  $\alpha\alpha$ -term in  $\bar{J}_{non\_loc\_2}$  is the  $\alpha$ -term in  $\bar{J}_{non\_loc\_1}$ ).

Minimization of the pseudo potential is performed by a finite element method using piecewise linear elements to interpolate  $\bar{\mathbf{v}}$  and  $\bar{\gamma}^\alpha$  fields and 100 nodes. Boundary conditions are imposed through penalization terms added to the potential. Namely, the term for velocities reads:

$$(2.50) \quad \begin{aligned} \bar{J}_{bond\_u}(\bar{\mathbf{v}}) &= \mathfrak{R}_u ((\bar{v}_x(\bar{y} = 0))^2 + (\bar{v}_x(\bar{y} = 1) - \dot{U})^2 + (\bar{v}_y(\bar{y} = 0))^2 + (\bar{v}_y(\bar{y} = 1))^2). \end{aligned}$$

Following (2.42)<sub>1</sub>, the term for slip rates is, for the *M1 model*:

$$(2.51) \quad \bar{J}_{bond\_r}(\bar{\gamma}^\alpha) = \mathfrak{R}_\gamma \bar{L}^2 \sum_\alpha ((\bar{\gamma}^\alpha(\bar{y} = 0))^2 + (\bar{\gamma}^\alpha(\bar{y} = 1))^2) (\mathbf{m}^\alpha \cdot \mathbf{e}_y)^2.$$

Following (2.42)<sub>2</sub>, for the *M2 model*:

$$\begin{aligned}
 (2.52) \quad \bar{J}_{bond-\gamma}(\bar{\gamma}^\alpha) &= \mathfrak{R}_\gamma \bar{L}^2 \left( \left\| \sum_{\alpha} \bar{\gamma}^\alpha(\bar{y} = 0) (\mathbf{n}^\alpha \cdot \mathbf{e}_x) \mathbf{m}^\alpha \otimes \mathbf{e}_z \right\|^2 \right. \\
 &\quad \left. + \left\| \sum_{\alpha} \bar{\gamma}^\alpha(\bar{y} = 1) (\mathbf{n}^\alpha \cdot \mathbf{e}_x) \mathbf{m}^\alpha \otimes \mathbf{e}_z \right\|^2 \right) \\
 &= \mathfrak{R}_\gamma \bar{L}^2 \left( \sum_{\alpha, \beta} \bar{\gamma}^\alpha(\bar{y} = 0) \bar{\gamma}^\beta(\bar{y} = 0) (\mathbf{n}^\alpha \cdot \mathbf{e}_x) (\mathbf{m}^\alpha \cdot \mathbf{m}^\beta) (\mathbf{n}^\beta \cdot \mathbf{e}_x) \right. \\
 &\quad \left. + \sum_{\alpha, \beta} \bar{\gamma}^\alpha(\bar{y} = 1) \bar{\gamma}^\beta(\bar{y} = 1) (\mathbf{n}^\alpha \cdot \mathbf{e}_x) (\mathbf{m}^\alpha \cdot \mathbf{m}^\beta) (\mathbf{n}^\beta \cdot \mathbf{e}_x) \right).
 \end{aligned}$$

In Eqs. (2.50), (2.51) and (2.52),  $\mathfrak{R}_u$  and  $\mathfrak{R}_\gamma$  are non-dimensional penalty parameters of high values. Minimization yields  $\bar{v}_x$ ,  $\bar{v}_y$  and  $\bar{\gamma}^\alpha$  on the nodes<sup>7</sup> and  $\bar{\rho}_e^\alpha$  and  $\bar{\tau}_b^\alpha$  are derived by finite difference evaluation of the gradients of  $\bar{\gamma}^\alpha$ .

### 3. Plastic slip profiles in a sheared band

This section investigates the incidence of non-local effects coupled with confined plasticity (micro-hard boundary conditions) on the selection of slip systems in the band. Namely, three systems with orientations close to the shear orientation (labelled by the angles  $\theta_\alpha$  formed with direction  $x$ ) are supposed to be potentially active at a time  $t = 0$ . The angles  $\theta_1$  and  $\theta_3$  are positive and  $\theta_2$  is negative (cf. Fig. 1):

$$(3.1) \quad \mathbf{m}^\alpha = \cos(\theta_\alpha) \mathbf{e}_x + \sin(\theta_\alpha) \mathbf{e}_y \quad \text{and} \quad \mathbf{n}^\alpha = -\sin(\theta_\alpha) \mathbf{e}_x + \cos(\theta_\alpha) \mathbf{e}_y,$$

with:  $\theta_1 = \pi/7$ ,  $\theta_2 = -\pi/12$  and  $\theta_3 = \pi/8$ .

One could easily establish that two slip systems with angles of opposite sign are enough to accommodate a shear deformation. In other words, systems 1 and 3 are redundant from a kinematic point of view.

The incremental problem is solved by minimizing the pseudo potential  $\bar{J}(\bar{\mathbf{v}}, \bar{\gamma}^\alpha)$ . The slip rate profiles obtained for local and non-local constitutive models are compared by using successively the *M1 model* and the *M2 model*. The local model leads to the formation of uniform slip rate profiles in the layer, the intensity of the different slip rates depending on the orientation of the slip systems on the one hand, and the latent-to-self-hardening ratios, on the other hand.

Due to micro-hard boundary conditions, for non-local models, in most cases (but not all of them as we see in Section 3.3), plastic slip rates annihilate for

<sup>7</sup>It is achieved by a Mathematica routine applied to the vectors of components of  $\bar{v}_x$ ,  $\bar{v}_y$  and  $\bar{\gamma}^\alpha$  on the shape functions.

$\bar{y} = 0$  and  $\bar{y} = 1$  and plastic slip concentrates in the center of the band, thus forming non-uniform profiles in the thickness. In other words, limit layers form near the boundaries in which plastic slip evolves from zero to nearly constant values; when the characteristic length of non-local effects is increased, the two limit layers tend to meet in the center and slip system activity is controlled by the boundary conditions.

In Section 3.1, all latent to self-hardening ratios are set equal and less than unity. As we shall see, for the local model, this situation favors the co-activation of the three systems even though two of them would be sufficient. The *M1 model* and *M2 model* modify this selection in the limit layer in a different way. In Section 3.2, two situations are considered in which the latent to self-hardening ratios are not equal and enhance activation of system 1 even though system 3 is the most favorably oriented towards the shear direction. At last, in Section 3.3, latent to self hardening ratios are the same as in Section 3.1 but system 3 is replaced by its orthogonal counterpart (the slip plane normal becomes the slip direction and vice-versa). Although the solution is identical in the local case, the gradient effects are substantially different than for the case of Section 3.1; moreover, the *M1 model* and *M2 model* give totally different activation profiles in the band thickness.

In the following, the non-dimensional parameters are set equal to the following:

$$\bar{\lambda} = 1.5 \quad \text{and} \quad \bar{H} = 0.05.$$

### 3.1. Low equal latent to self hardening ratios

The three latent to self hardening ratios are first supposed to be the same and lower than unity:  $q_{12} = q_{23} = q_{31} = 0.5$ . For the local model, the slip rates are respectively  $\bar{\gamma}^1 = 0.15$ ,  $\bar{\gamma}^2 = 0.67$  and  $\bar{\gamma}^3 = 0.32$ , in accordance with  $|\theta_1| > |\theta_3| > |\theta_2|$  namely with the more or less favorable orientation of the system towards the shear direction. The slip rates given by the *M1 model* and a characteristic length  $\bar{L} = 0.1$  are nearly homogeneous in the center of the band and the profiles exhibit a transition from zero in the limit layer for the three systems (Fig. 2a). The order of the three slip rates is not modified. When the characteristic length is raised up to 0.5, the two limit layers enlarge and meet in the center, the three slip rate profiles forming bell-shaped curves (Fig. 2b) as has already been observed in double slip simulations [31]. The rates of dislocation density are reported in Fig. 3: for  $\bar{L} = 0.1$ , polar dislocations concentrate near the boundaries (Fig. 3a) whereas for  $\bar{L} = 0.5$  these densities evolve almost linearly in the band thickness (Fig. 3b). Figure 4 displays the profiles for the rates of critical shear stress, back stress and resolved shear stress for system 1 and the two values of  $\bar{L}$ . For  $\bar{L} = 0.1$ , the rate of the back stress annihilates in the center

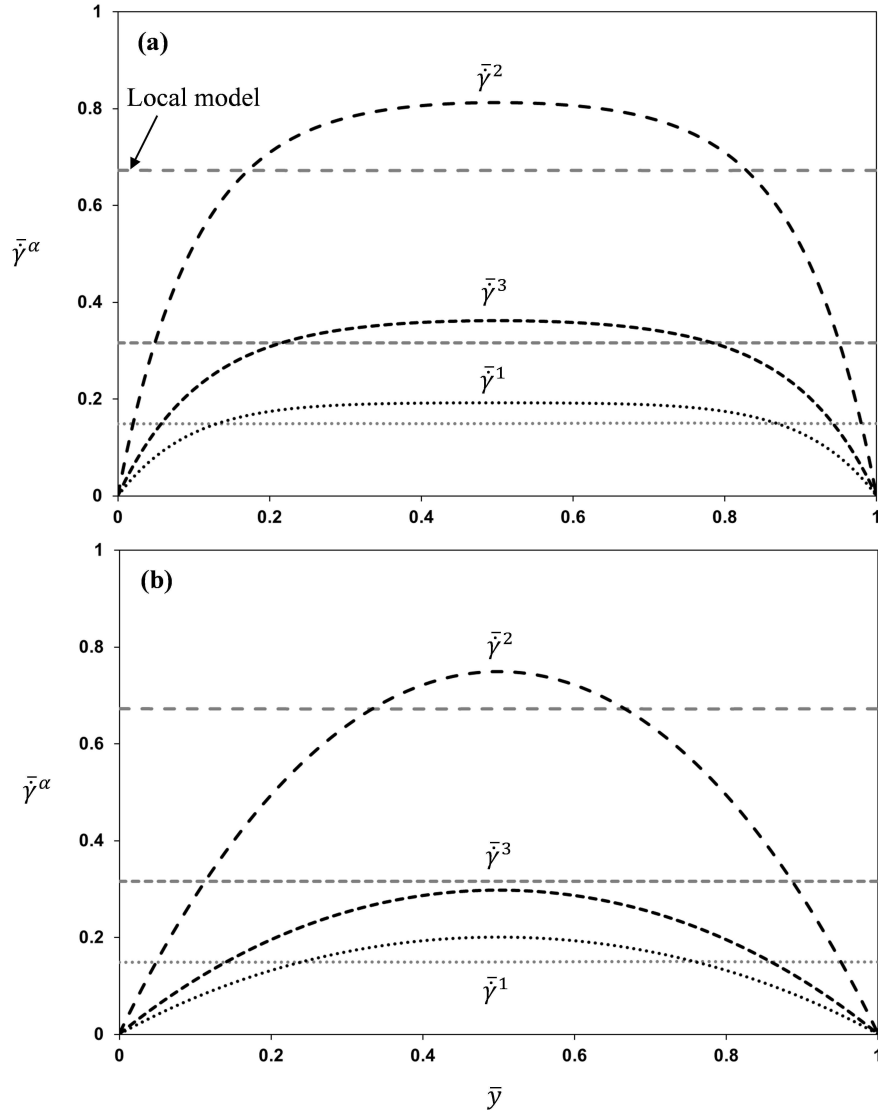


FIG. 2. Slip rate profiles for the three slip systems for the local model (dark gray lines) and *M1 model* (black lines) and a characteristic length (a)  $\bar{L} = 0.1$  and (b)  $\bar{L} = 0.5$ .

of the band where non-local effects are therefore negligible (Fig. 4a); it increases in the limit layer while the rate of critical shear stress tends to zero. For  $\bar{L} = 0.5$ , the rate of the back stress dominates the rate of the critical shear stress in the whole band (Fig. 4b): in other words, the slip activity is mainly controlled by non-local effects in this case.

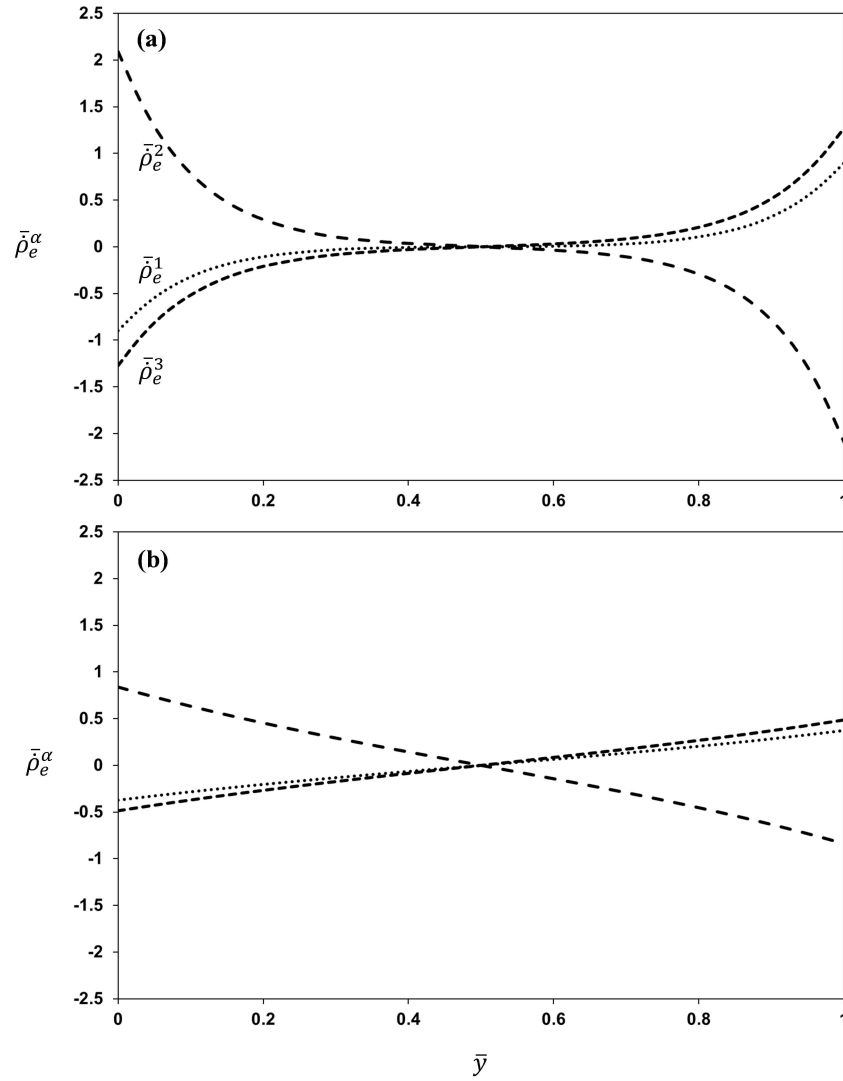


FIG. 3. Dislocation density profiles for the three slip systems for the *M1 model* and a characteristic length (a)  $\bar{L} = 0.1$  and (b)  $\bar{L} = 0.5$ .

For the *M2 model* and the characteristic length  $\bar{L} = 0.1$ , the structure of the limit layer is substantially different with non-coexistence of gradients for systems 1 and 3 (Fig. 5a): namely, in the first part  $\bar{\gamma}^3$  evolves from zero to a constant value and  $\bar{\gamma}^1$  remains zero; in a second part,  $\bar{\gamma}^1$  evolves and reaches a nearly constant value while it approaches the center of the band. Let us recall that the change from the *M1 model* to the *M2 model* introduces coupling terms between

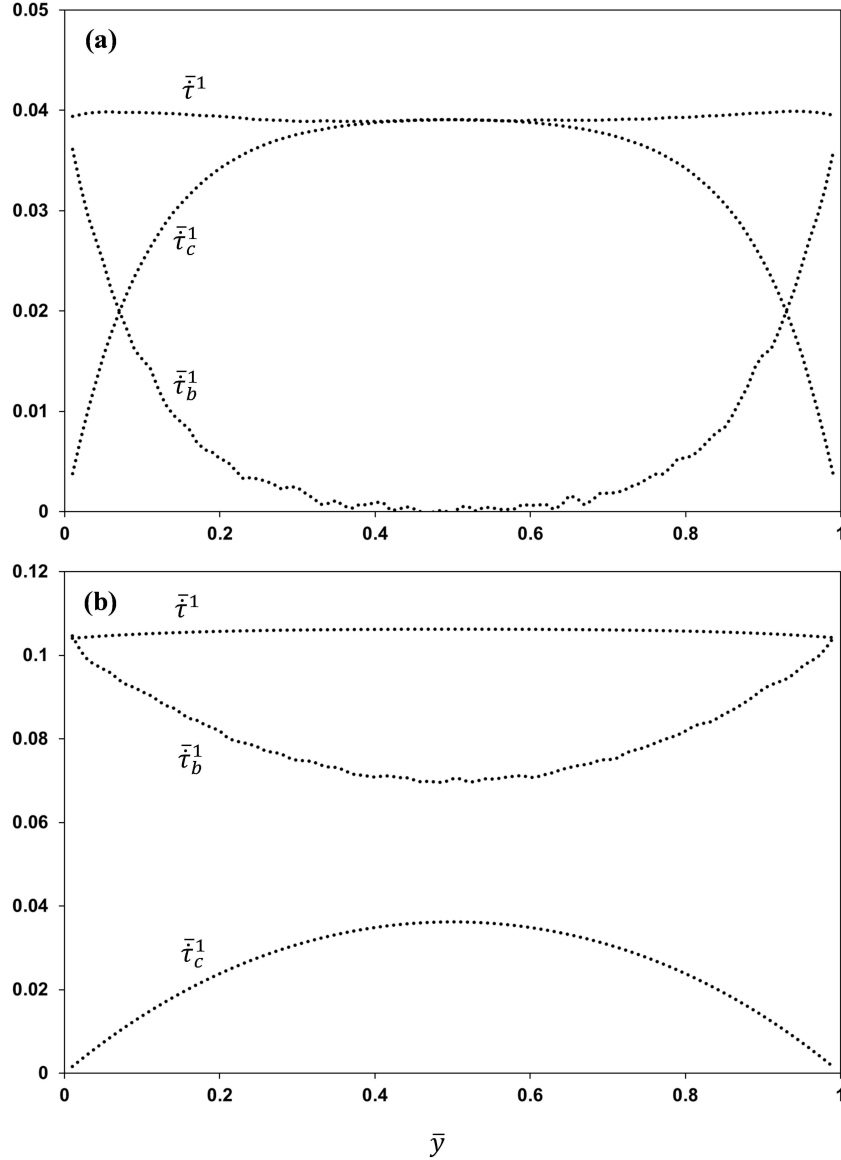


FIG. 4. Rate of critical shear stress, back stress and resolved shear stress for system 1 for the *M1 model* and a characteristic length (a)  $\bar{L} = 0.1$  and (b)  $\bar{L} = 0.5$ .

the gradients of slips of the different systems according to Eq. (2.45)<sub>2</sub>. Following the sign of  $(\mathbf{n}^\alpha \cdot \mathbf{e}_x)(\mathbf{n}^\beta \cdot \mathbf{e}_x)$ , these  $\alpha\beta$ -terms favor coexistence of gradients of the same sign for  $\bar{\gamma}^1$  and  $\bar{\gamma}^2$ , and  $\bar{\gamma}^3$  and  $\bar{\gamma}^2$  but penalizes such coexistence for  $\bar{\gamma}^1$  and  $\bar{\gamma}^3$ . Since  $(\mathbf{n}^1 \cdot \mathbf{e}_x)^2 > (\mathbf{n}^3 \cdot \mathbf{e}_x)^2$ , system 3 is favored in the first part of the limit layer in which gradients are the strongest. For  $\bar{L} = 0.5$ , the *M2 model*

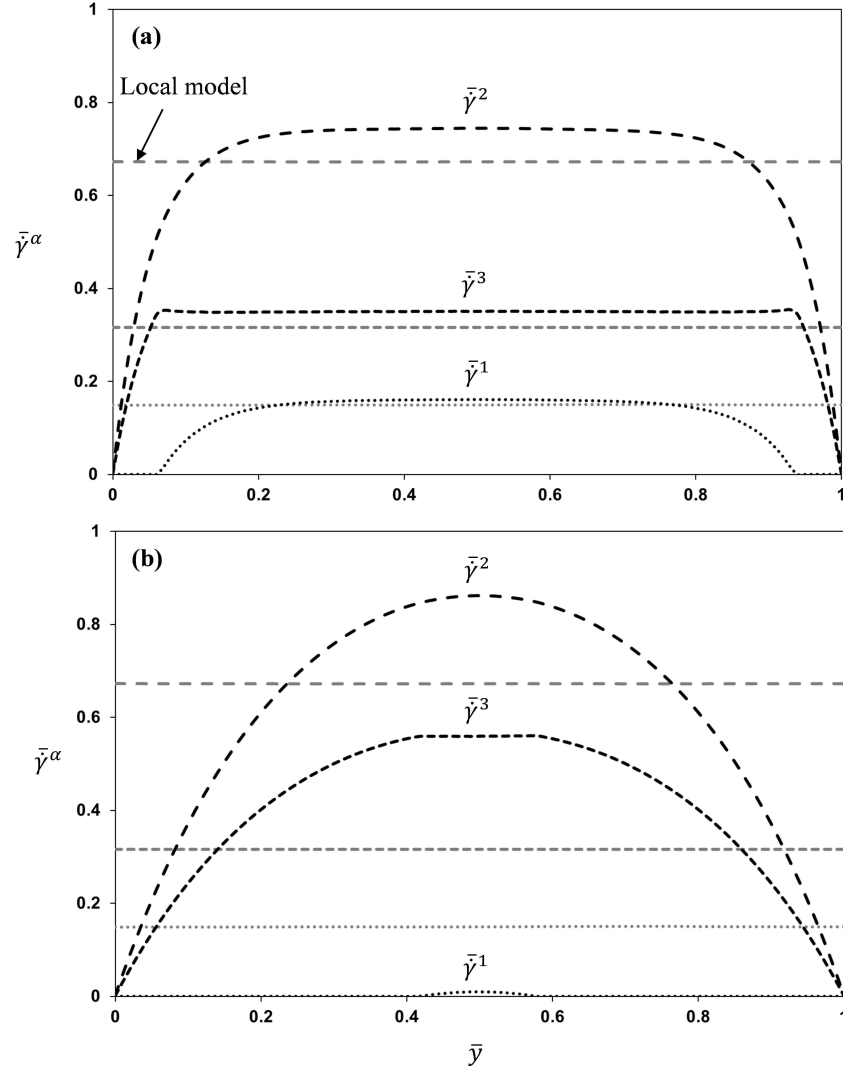


FIG. 5. Slip rate profiles for the three slip systems for the local model (dark gray lines) and *M2 model* (black lines) and a characteristic length (a)  $\bar{L} = 0.1$  and (b)  $\bar{L} = 0.5$ .

leads to complete extinction of system 1 (Fig. 5b). The norm of the dislocation density tensor rate  $\|\dot{\bar{\mathbf{G}}}\| = \sqrt{\dot{\bar{\mathbf{G}}} : \dot{\bar{\mathbf{G}}}}$  is reported in Fig. 6 for the two characteristic lengths: as for the rate of dislocation densities with the *M1 model*, it concentrates near the boundaries for  $\bar{L} = 0.1$  and is positive in the whole band for  $\bar{L} = 0.5$ . The shear stress profiles of system 1 (Fig. 7) exhibit a back stress higher than the resolved shear stress near the boundaries which justifies extinction of system 1. In other words, although latent hardening would favor coexistence of the three

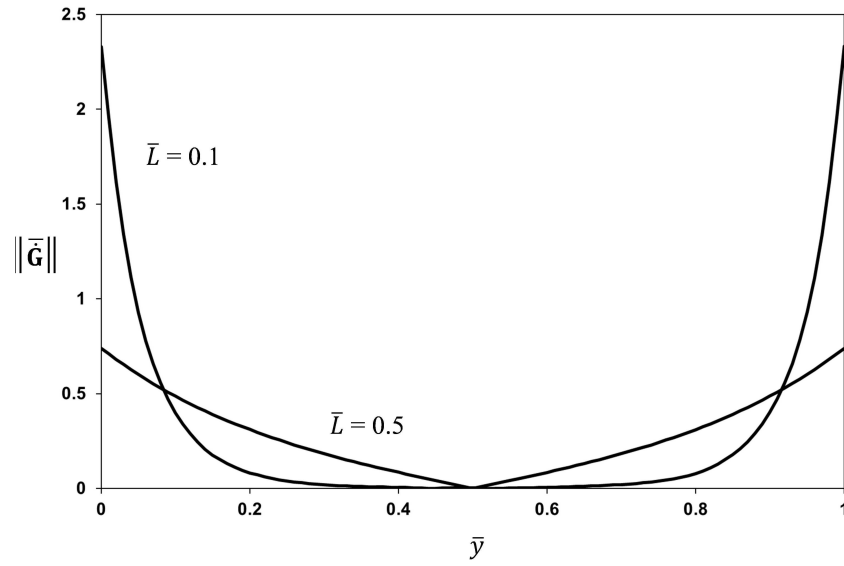


FIG. 6. Norm of the dislocation density tensor rate for the *M2 model* for characteristic lengths  $\bar{L} = 0.1$  and  $\bar{L} = 0.5$ .

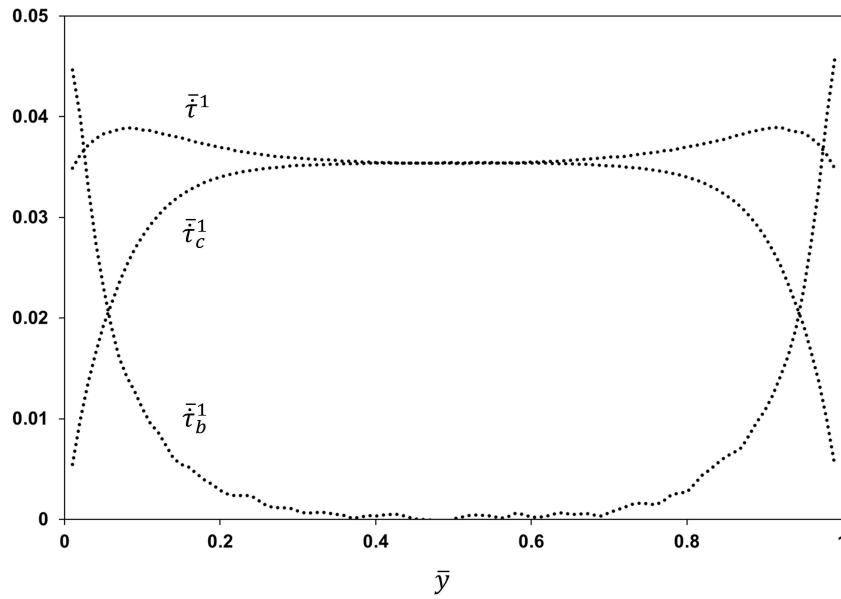


FIG. 7. Rate of critical shear stress, back stress and resolved shear stress for system 1 for the *M2 model* and a characteristic length  $\bar{L} = 0.1$ .

systems, gradient plasticity effects progressively induce selection of systems 2 and 3 alone.

### 3.2. Unequal latent to self hardening ratios favoring system 1

In this subsection, two cases are investigated for which latent to self-hardening ratios tend to favor system 1 even though its orientation is less favorable than the one of system 3.

In the first case, all ratios are assumed below 1 but  $q_{12}$  is assumed to be lower than the two others ( $q_{12} = 0.25$  and  $q_{23} = q_{31} = 0.5$ ). For the local model, the slip rates are respectively  $\bar{\gamma}^1 = 0.32$ ,  $\bar{\gamma}^2 = 0.70$  and  $\bar{\gamma}^3 = 0.14$ . With the *M1*

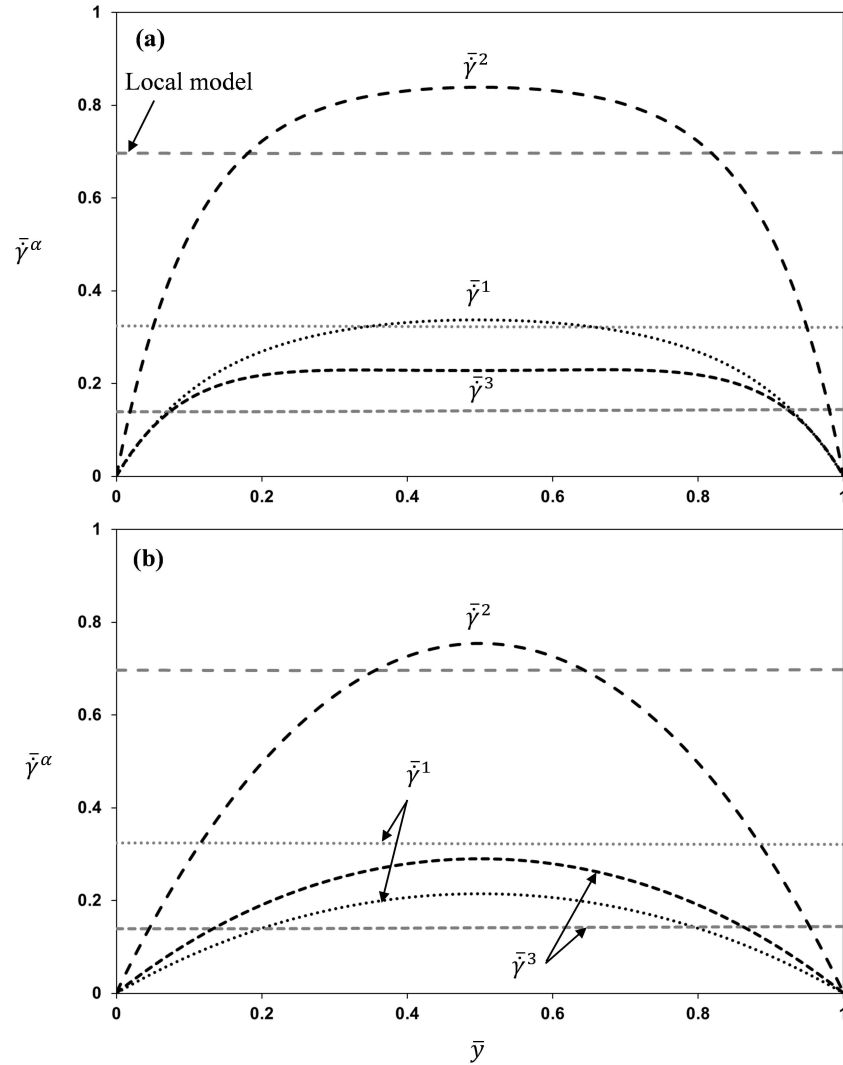


FIG. 8. Slip rate profiles for the three slip systems for the local model (dark gray lines) and *M1 model* (black lines), a latent to self hardening ratio  $q_{12} = 0.25$  and a characteristic length (a)  $\bar{L} = 0.1$  and (b)  $\bar{L} = 0.5$ .

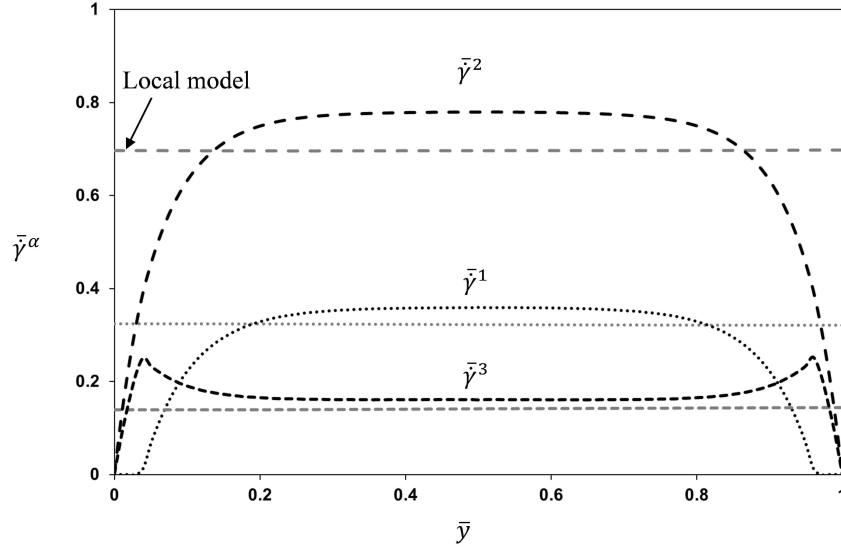


FIG. 9. Slip rate profiles for the three slip systems for the local model (dark gray lines) and *M2 model* (black lines), a latent to self hardening ratio  $q_{12} = 0.25$  and a characteristic length  $\bar{L} = 0.1$ .

*model*, the increase of  $\bar{L}$  progressively penalizes system 1 (Fig. 8) in accordance with  $(\mathbf{n}^1 \cdot \mathbf{e}_x)^2 > (\mathbf{n}^3 \cdot \mathbf{e}_x)^2$ . For  $\bar{L} = 0.1$ ,  $\bar{\gamma}^1 \approx \bar{\gamma}^3$  near the boundaries whereas it is still higher in the center and the transition zone is larger for system 1 (Fig. 8a). For  $\bar{L} = 0.5$ , system 3 now dominates system 1 in the whole band and the slip rate profiles are nearly identical than the ones obtained for the case with three equal latent to self-hardening ratios (Fig. 8b vs Fig. 2b); in other words, for high  $\bar{L}$ , the role of latent hardening becomes negligible which is consistent with the prominence of back stresses on critical shear stresses. For the *M2 model*, a double limit layer structure is still displayed with system 3 alone in a first part of the limit layer (Fig. 9). In the second part, systems 1 and 3 exhibit gradients of opposite sign. The increase of  $\bar{L}$  progressively leads to the extinction of system 1 (but for a value of  $\bar{L}$  above 0.5 not represented here).

In a second case, the latent to self-hardening ratio for systems 2 and 3 is supposed to be higher than unity, the other ones being kept lower:  $q_{12} = q_{31} = 0.5$  and  $q_{23} = 1.2$ . In this case, due to the redundancy of system 1 and 3, the local model predicts non activation of system 3 balanced by a higher activation of system 1 (even though system 3 is the most favorably oriented of the two):  $\bar{\gamma}^1 = 0.44$ ,  $\bar{\gamma}^2 = 0.71$  and  $\bar{\gamma}^3 = 0$ . The increase of non-local effects progressively re-activates system 3. For the *M1 model*, the coexistence of systems 1 and 3 is restored (Fig. 10), starting from the boundaries. The slip rate gradients being uncoupled, non-local effects favor distribution of plastic slip gradients on the

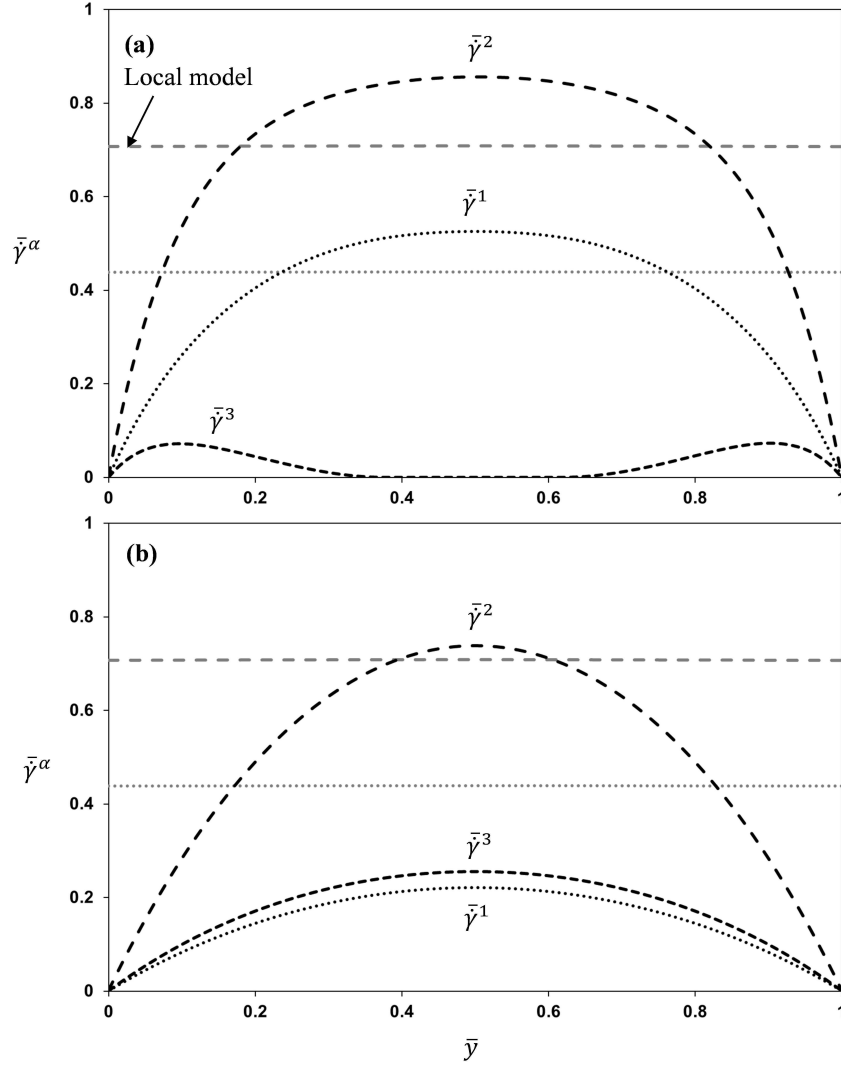


FIG. 10. Slip rate profiles for the three slip systems for the local model (dark gray lines) and *M1 model* (black lines), a latent to self hardening ratio  $q_{23} = 1.2$  and a characteristic length (a)  $\bar{L} = 0.1$  and (b)  $\bar{L} = 0.5$ .

two systems. For  $\bar{L} = 0.5$ ,  $\bar{\gamma}^1 \approx \bar{\gamma}^3$  which emphasizes once again the first order influence of gradient effects, the slip rate profiles being close to the ones obtained with the other latent to self-hardening ratios. For the *M2 model*, system 3 is still re-activated in the limit layer and system 1 is de-activated in a first part where the slip gradient for system 3 is positive. In a second part of the limit layer, systems 1 and 3 coexist with gradients of opposite sign (Fig. 11). In the center

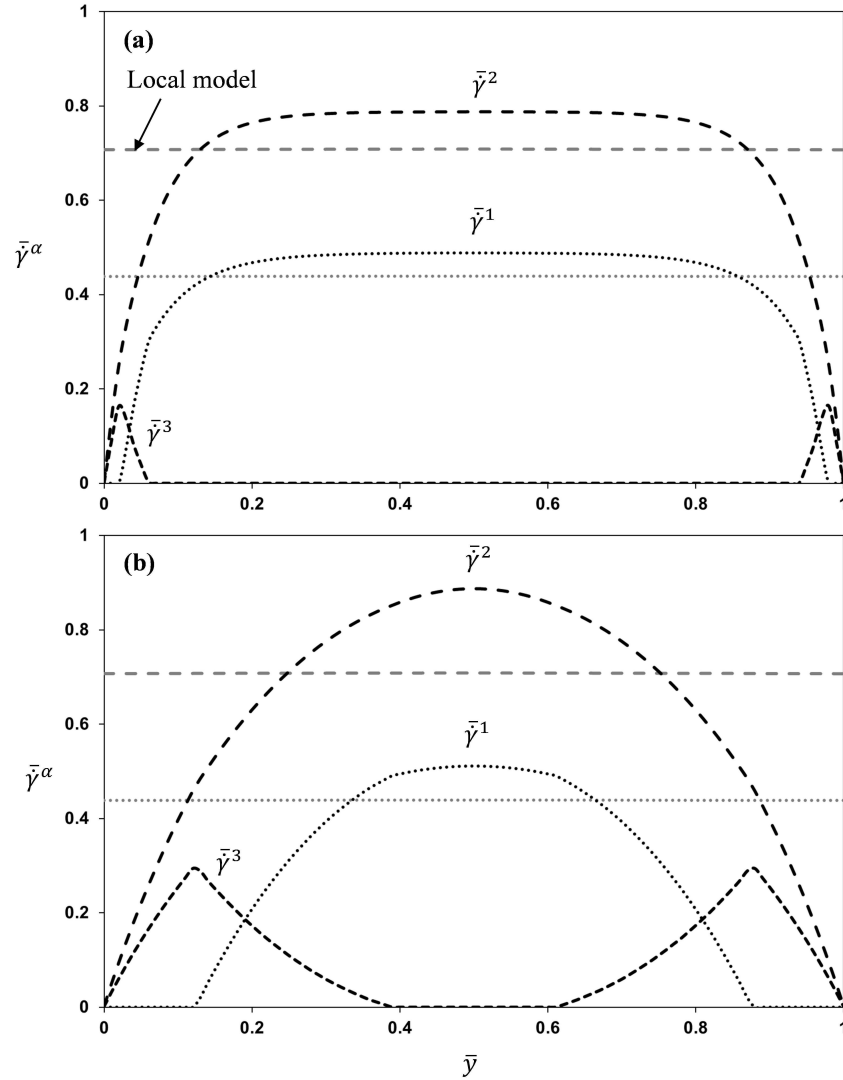


FIG. 11. Slip rate profiles for the three slip systems for the local model (dark gray lines) and *M2 model* (black lines), a latent to self hardening ratio  $q_{23} = 1.2$  and a characteristic length (a)  $\bar{L} = 0.1$  and (b)  $\bar{L} = 0.5$ .

of the band, systems 1 and 2 remain alone consistently with latent hardening penalizing system 3.

### 3.3. One “orthogonal” slip system

In this subsection, system 3 is replaced by its orthogonal counterpart system 3\*, i.e. the slip plane normal  $\mathbf{n}^3$  and the slip direction  $\mathbf{m}^3$  are exchanged, the

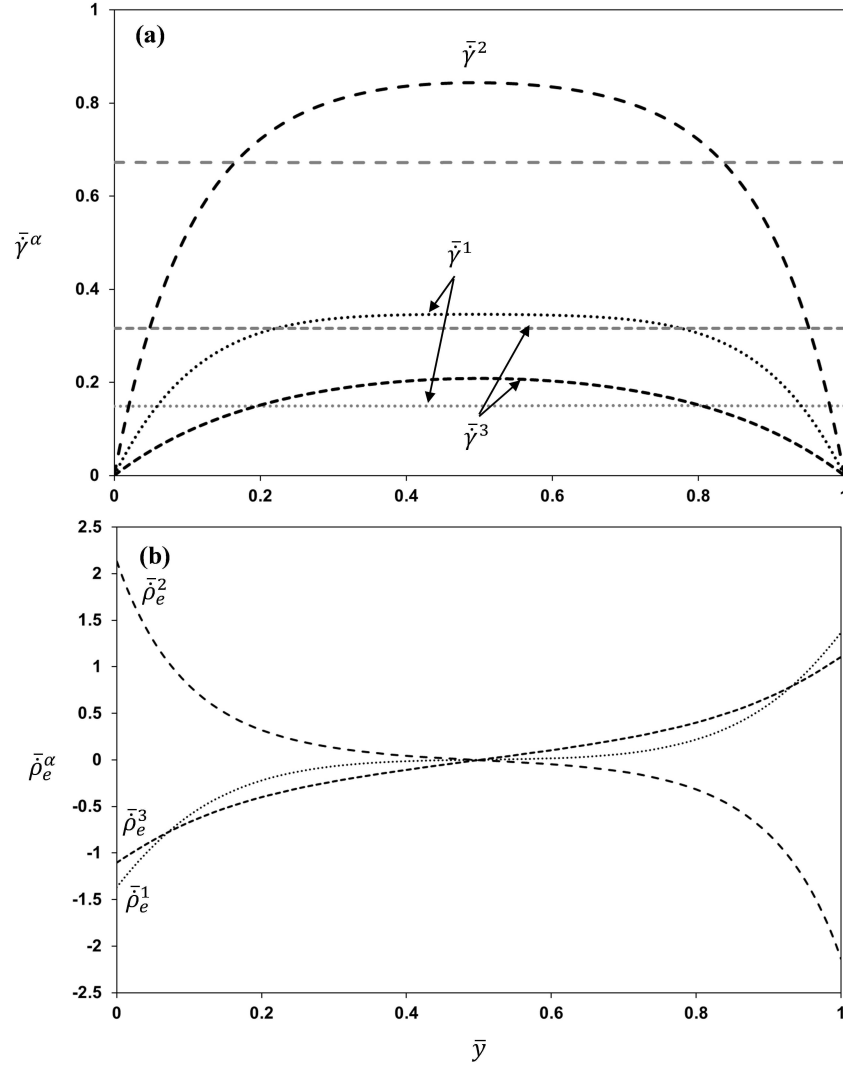


FIG. 12. (a) Slip rate and (b) dislocation density profiles for the three slip systems 1, 2 and 3\* for the local model (dark gray lines) and *M1 model* (black lines) and a characteristic length  $\bar{L} = 0.1$ .

former being now close to the shear direction. Low equal latent to self-hardening ratios are kept as in the case of Section 3.1 ( $q_{12} = q_{23*} = q_{3*1} = 0.5$ ). For the local model and a small deformation theory, these two cases are strictly identical<sup>8</sup> and lead to the same slip rates ( $\bar{J}_{loc}(\bar{\mathbf{v}}, \bar{\gamma}^\alpha)$  only depends on the symmetric parts of the outer products  $\mathbf{m}^\alpha \otimes \mathbf{n}^\alpha$ ).

<sup>8</sup>This would not be the case in a finite deformation framework due to the rotation of slip systems as shown in ASARO [44] for instance.

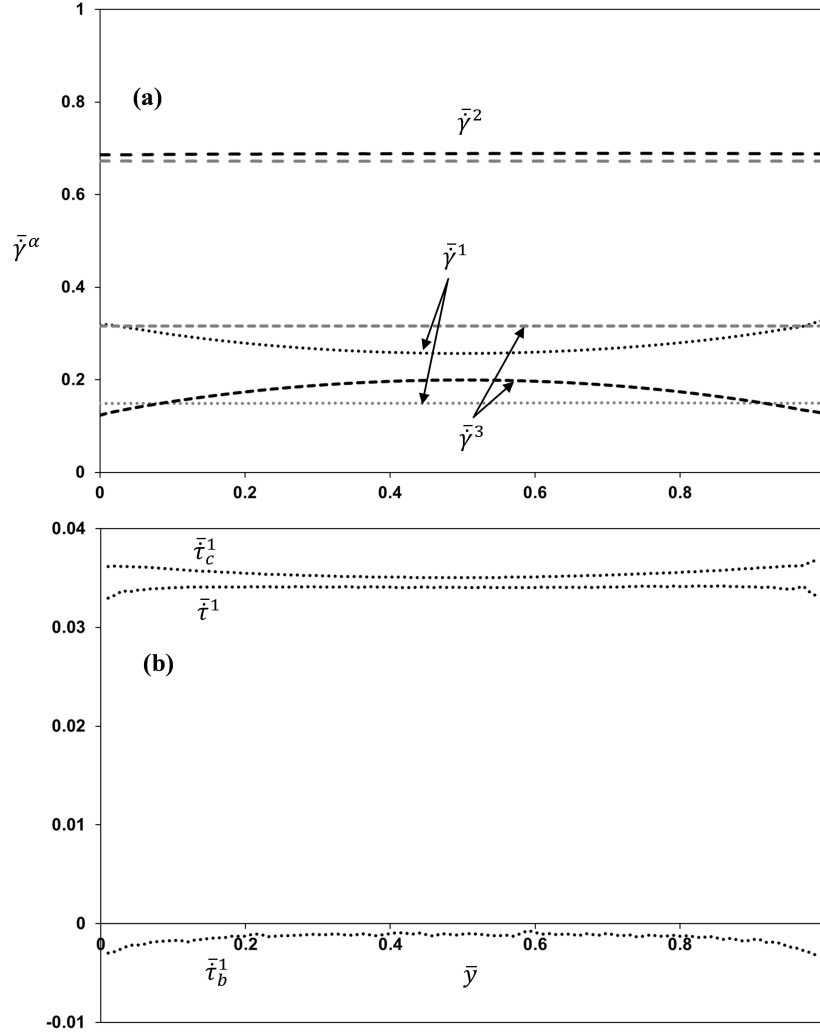


FIG. 13. (a) Slip rate profiles for the three slip systems 1, 2 and 3\* for the local model (dark gray lines) and  $M2$  model (black lines) and a characteristic length  $\bar{L} = 0.1$ . (b) Rate of critical shear stress, back stress and resolved shear stress for system 1 for the  $M2$  model.

However, with the  $M1$  model, the non-local effects are far much stronger for system 3\* than for system 3 in accordance with  $(\mathbf{n}^{3*} \cdot \mathbf{e}_x)^2 = (\mathbf{m}^3 \cdot \mathbf{e}_x)^2 \gg (\mathbf{n}^3 \cdot \mathbf{e}_x)^2$  (namely, the slip plane of system 3\* is almost perpendicular to the boundaries). This is consistent with the results established for kink band formation by FOREST [45] for instance. Till  $\bar{L} = 0.1$  the order of slip rates for system 1 and 3\* is inverted in comparison with the local case (Fig. 12a), system 1 being strongly enhanced. Although the increase of dislocation densities  $\bar{\rho}_e^1$  and  $\bar{\rho}_e^2$  concentrates near the boundaries,  $\bar{\rho}_e^{3*}$  spreads in the whole band (Fig. 12b).

The *M2 model* displays a totally different behavior since, in  $\bar{y} = 0$  and  $\bar{y} = 1$ , annihilation of the density tensor flow does not yield annihilation of the three slip rates as is seen on the slip rate profiles of Fig. 13a. Non-local effects enhance the slip rate  $\bar{\gamma}^1$  and reduces the slip rate  $\bar{\gamma}^3$  when going from the center to the boundaries. Since  $(\mathbf{n}^{3*} \cdot \mathbf{e}_x)(\mathbf{n}^1 \cdot \mathbf{e}_x) \geq 0$ , non local effects favor gradients of opposite sign for the two systems. The shear stress profiles of system 1 (Fig. 13b) exhibit a negative back stress which justifies the fact that  $\bar{\gamma}^1$  is higher than in the local model case.

#### 4. Concluding remarks

The combination of gradient plasticity effects with extended boundary conditions modifies the activation of slip systems in a single crystal of a finite size. Namely, non-local formulations introduce a characteristic length scale which controls the extent of a limit layer near boundaries in which system selection may be different from the bulk. When this length scale is of the same order as the size of the single crystal, gradient effects drive activation all over it. These phenomena have been illustrated by considering the classical bi-dimensional model of a band of finite thickness submitted to a simple shear deformation and micro-hard boundary conditions simulating the behavior of a grain boundary interface. Assuming that non-local plasticity effects stem from the storage of polar dislocation densities, two formulations have been tested for the defect energy: the first one is proportional to the square of polar edge densities for all systems (*M1 model*) and the second one is a quadratic form of the dislocation density tensor (*M2 model*).

Since these two formulations give substantially different behaviors in some cases, their physical justification in the context of grain boundary interfaces needs to be examined. A few elements are given in NICOLA *et al.* [46], although their analysis deals with an interface between a thin film and a substrate and not with a crystal in an aggregate. The *M1 model* assumes that the accumulation of polar densities proceeds independently on the different systems and the defect energy would be the one of dislocation pile-ups, the interactions between pile-ups from the different slip systems being negligible. In micro-hard conditions, no dislocation of any system can cross grain boundaries. On the contrary, the *M2 model* postulates that the defect energy is the same for all polar dislocation arrangements leading to a given net Burgers vector regardless of the slip systems they come from. In the rigid plastic limit case, namely for  $\boldsymbol{\varepsilon}^e = 0$ , the defect energy is a function of the lattice curvature (the relation between the dislocation density tensor and the curvature tensor is established in FRESSENGEAS *et al.* [47] for instance). In micro-hard conditions, dislocation flows are allowed through the boundaries provided that the Burgers vector flow is zero (in the rigid plastic

case, this condition amounts to constant lattice misorientation between the two grains [36]).

For the *M2 model*, weaker grain boundary constraints were next proposed by GURTIN [48] who defined a surface dislocation density tensor to which additional defect energy is related. The evolution of this tensor equals the net Burgers vector flow and the possibility to accumulate GND on the boundary is assumed. Slip system activity and the role of both volume and surface defect energy on system selection could be investigated in this framework. However, the grain boundary approach of [48] should be brought together with the modelling of the intrinsic structure of grain boundaries. Namely, the former are represented as structured dislocation networks pre-existing to deformation which accommodate the lattice incompatibility between the two grains (see VATTRE and DEMKOWICZ [49] for instance). These dislocations must contribute to the defect energy and may interact with GND stored during deformation.

## References

1. U.F. KOCKS, *Polyslip in single crystals*, Acta Metallurgica, **8**, 345–352, 1960.
2. P. FRANCIOSI, A. ZAOU, *Multislip tests on copper crystals: a junctions hardening effect*, Acta Metallurgica, **30**, 2141–215, 1982.
3. G.R. PIERCY, R.W. CAHN, A.H. COTTRELL, *A study of primary and conjugate slip in crystals of alpha brass*, Acta Metallurgica, **3**, 331–338, 1955.
4. S. SAIMOTO, *Low Temperature Tensile Deformation of Copper Single Crystals Oriented for Multislip*, PhD Thesis, M.I.T., Cambridge, Massachusetts, 1960.
5. O. DMITRIEVA, P.W. DONDL, S. MULLER, D. RAABE, *Lamination microstructure in shear deformed copper single crystals*, Acta Materialia, **57**, 3439–3444, 2009.
6. T. YALCINKAYA, W.A.M. BREKELMANS, M.G.D. GEERS, *Non-convex rate dependent strain gradient crystal plasticity and deformation patterning*, International Journal of Solids and Structures, **49**, 2625–2636, 2012.
7. J.L. DEQUIEDT, C. DENOVAL, R. MADEC, *Heterogeneous deformation in ductile fcc single crystals in biaxial stretching: the influence of slip system interactions*, Journal of Mechanics and Physics of Solids, **83**, 301–318, 2015.
8. D. WANG, M. DIEHL, F. ROTERS, D. RAABE, *On the role of the collinear dislocation interaction in deformation patterning and laminate formation in single crystal plasticity*, Mechanics of Materials, **125**, 70–79, 2018.
9. B. KLUSEMANN, T. YALCINKAYA, M.G.D. GEERS, B. SVENDSEN, *Application of non-convex rate dependent gradient plasticity to the modelling and simulation of inelastic microstructure development and inhomogeneous material behavior*, Computational Materials Science, **80**, 51–60, 2013.
10. G. LANCIONI, G. ZITTI, T. YALCINKAYA, *Rate independent deformation patterning in crystal plasticity*, Key Engineering Materials, **651-653**, 944–949, 2015.

11. Q.S. NGUYEN, *Bifurcation and stability of time independent standard dissipative systems*, [in:] Q.S. Nguyen [ed.], *Bifurcation and Stability of Dissipative Systems*, CISM Courses and Lectures **327**, International Center for Mechanical Science, Springer, Vienna, pp. 45–94, 1993.
12. M. ORTIZ, E.A. REPETTO, *Nonconvex energy minimization and dislocation structures in ductile single crystals*, *Journal of Mechanics and Physics of Solids*, **47**, 397–462, 1999.
13. B. BOURDIN, G. FRANCFORT, J.J. MARIGO, *The variational approach to fracture*, *Journal of Elasticity*, **91**, 5–148, 2008.
14. K. PHAM, H. AMOR, J.J. MARIGO, C. MAURINI, *Gradient damage models and their use to approximate brittle fracture*, *International Journal of Damage Mechanics*, **20**, 618–652, 2011.
15. H. PETRYK, M. KURSA, *The energy criterion for deformation banding in ductile single crystals*, *Journal of Mechanics and Physics of Solids*, **61**, 1854–1875, 2013.
16. H. PETRYK, M. KURSA, *Incremental work minimization algorithm for rate independent plasticity of single crystals*, *International Journal for Numerical Methods in Engineering*, **104**, 157–184, 2015.
17. M. ORTIZ, E.A. REPETTO, L. STAINIER, *A theory of subgrain dislocation structures*, *Journal of Mechanics and Physics of Solids*, **48**, 2077–2114, 2000.
18. J. KRATOCHVIL, M. KRUZIK, *A crystal plasticity model of a formation of a deformation band structure*, *Philosophical Magazine*, **95**, 32, 3621–3639, 2015.
19. D. PEIRCE, R.J. ASARO, A. NEEDLEMAN, *An analysis of non-uniform and localized deformation in ductile single crystals*, *Acta Metallurgica*, **30**, 1087–1119, 1982.
20. G. LANCIONI, T. YALCINKAYA, A. COCKS, *Energy-based non-local plasticity models for deformation patterning, localization and fracture*, *Proceedings of the Royal Society A*, **471**, 275, 2015.
21. A. MOLINARI, *Shear bands in a viscoplastic single crystal in tension*, *Proceedings of the Academy of Sciences, Paris*, **306**, Série II, 841–846, 1988.
22. L. KUBIN, B. DEVINCRE, T. HOC, *Modelling dislocation storage rates and mean free paths in face-centered cubic crystals*, *Acta Materialia*, **56**, 6040–6049, 2008.
23. C. TEODOSIU, J.L. RAPHAEL, L. TABOUROT, *Finite element simulation of the large elastoplastic deformation*, [in:] C. Teodosiu, J.L. Raphanel and F. Sidoroff, *Large Plastic Deformations*, Balkema, Rotterdam, 1991.
24. J.L. DEQUIEDT, *The incidence of slip system interactions on the deformation of FCC single crystals: system selection and segregation for local and non-local constitutive behavior*, *International Journal of Solids and Structures*, **141-142**, 1–14, 2018.
25. S. YEFIMOV, I. GROMA, E. VAN DER GIESSEN, *A comparison of a statistical-mechanics based plasticity model with discrete dislocation plasticity calculations*, *Journal of Mechanics and Physics of Solids*, **52**, 279–300, 2004.
26. L.P. EVERS, W.A.M. BREKELMANS, M.G.D. GEERS, *Scale dependent crystal plasticity framework with dislocation density and grain boundary effects*, *International Journal of Solids and Structures*, **41**, 5209–5230, 2004.

27. C.J. BAYLEY, W.A.M. BREKELMANS, M.G.D. GEERS, *A comparison of dislocation induced back stress formulations in strain gradient crystal plasticity*, International Journal of Solids and Structures, **43**, 7268–7286, 2006.
28. M. KURODA, V. TVERGAARD, *Studies of scale dependent crystal viscoplasticity models*, Journal of Mechanics and Physics of Solids, **54**, 1789–1810, 2006.
29. N.A. FLECK, G.M. MULLER, M.F. ASHBY, J.W. HUTCHINSON, *Strain gradient plasticity: theory and experiment*, Acta Metallurgica et Materialia, **42**, 2, 475–487, 1994.
30. H. GAO, Y. HUANG, W.D. NIX, J.W. HUTCHINSON, *Mechanism-based strain gradient plasticity – I. Theory*, Journal of Mechanics and Physics of Solids, **47**, 1239–1263, 1999.
31. L.P. EVERS, W.A.M. BREKELMANS, M.G.D. GEERS, *Non-local crystal plasticity model with intrinsic SSD and GND effects*, Journal of Mechanics and Physics of Solids, **52**, 2379–2401, 2004.
32. A. MA, F. ROTERS, D. RAABE, *A dislocation density based constitutive model for crystal plasticity FEM including geometrically necessary dislocations*, Acta Materialia, **54**, 2169–2179, 2006.
33. H. PETRYK, S. STUPKIEWICZ, *A minimal gradient enhancement of the classical continuum theory of crystal plasticity. Part I: the hardening law*, Archives of Mechanics, **68**, 6, 459–485, 2016.
34. M.E. GURTIN, *A gradient theory of single-crystal viscoplasticity that accounts for geometrically necessary dislocations*, Journal of Mechanics and Physics of Solids, **50**, 5–32, 2002.
35. I. ERTURK, J.A.W. VAN DOMMELEN, M.G.D. GEERS, *Energetic dislocation interactions and thermodynamical aspects of strain gradient crystal plasticity theories*, Journal of Mechanics and Physics of Solids, **57**, 1801–1814, 2009.
36. M.E. GURTIN, A. NEEDLEMAN, *Boundary conditions in small-deformation, single-crystal plasticity that account for the Burgers vector*, Journal of Mechanics and Physics of Solids, **53**, 1–31, 2005.
37. S. YEFIMOV, E. VAN DER GIESSEN, *Multiple slip in a strain-gradient plasticity model motivated by a statistical-mechanics description of dislocations*, International Journal of Solids and Structures, **42**, 3375–3394, 2005.
38. M.E. GURTIN, L. ANAND, S.P. LELE, *Gradient single-crystal plasticity with free energy dependent on dislocation densities*, Journal of Mechanics and Physics of Solids, **55**, 1853–1878, 2007.
39. J.F. NYE, *Some geometrical relations in dislocated solids*, Acta Metallurgica, **1**, 153–162, 1953.
40. P. CERMELLI, M.E. GURTIN, *On the characterization of geometrically necessary dislocations in finite plasticity*, Journal of Mechanics and Physics of Solids, **49**, 1539–1568, 2001.
41. A. ARSENLIS AND D.M. PARKS, *Crystallographic aspects of geometrically-necessary and statistically stored dislocation density*, Acta Materialia, **47**, 1597–1611, 1999.
42. N. OHNO, D. OKUMURA, *Higher-order stress and grain size effects due to self-energy of geometrically necessary dislocations*, Journal of Mechanics and Physics of Solids, **55**, 1879–1898, 2007.

43. I. GROMA, F.F. CSIKOR, M. ZAISER, *Spatial correlations and higher-order gradient terms in a continuum description of dislocation dynamics*, Acta Materialia, **51**, 1271–1281, 2003.
44. R.J. ASARO, *Micromechanics of crystals and polycrystals*, Advances in Applied Mechanics, **23**, 1–115, 1983.
45. S. FOREST, *Modeling slip, kink and shear banding in classical and generalized single crystal plasticity*, Acta Materialia, **46**, 9, 3265–3281, 1998.
46. L. NICOLA, E. VAN DER GIESSEN, M.E. GURTIN, *Effect of defect energy on strain gradient predictions of confined single crystal plasticity*, Journal of Mechanics and Physics of Solids, **53**, 1280–1294, 2005.
47. C. FRESSENGEAS, V. TAUPIN, L. CAPOLUNGO, *An elasto-plastic theory of dislocation and disclination fields*, International Journal of Solids and Structures, **48**, 3499–3509, 2011.
48. M.E. GURTIN, *A theory of grain boundaries that accounts automatically for grain misorientation and grain-boundary orientation*, Journal of Mechanics and Physics of Solids, **56**, 640–662, 2008.
49. A.J. VATTRE, M.J. DEMKOWICZ, *Determining the Burgers vectors and elastic strain energies of interface dislocation arrays using anisotropic elasticity theories*, Acta Materialia, **61**, 5172–5187, 2013.

Received October 12, 2018; revised version May 2, 2019.

Published online June 28, 2019.

---